12-2008

Modeling, Designing, Fabricating, and Testing of Channel Panel Flat Plate Heat Pipes

James R. Harris
Utah State University

MODELING, DESIGNING, FABRICATING, AND TESTING OF CHANNEL PANEL FLAT PLATE HEAT PIPES

by

James Harris

A thesis submitted in partial fulfillment
of the requirements for the degree

of

MASTER OF SCIENCE

in

Mechanical Engineering

Approved:

Dr. Leijun Li Major Professor	Dr. J. C. Batty Committe Member
Dr. Byard Wood Committee Member	Dr. Byron R. Burnham Dean of Graduate Studies

UTAH STATE UNIVERSITY
Logan, Utah

2008

Abstract

Modeling, Designing, Fabricating, and Testing of Channel Panel Flat Plate Heat Pipes

by

James R. Harris, Master of Science

Utah State University, 2008

Major Professor: Dr. Leijun Li
Department: Mechanical and Aerospace Engineering

Flat plate heat pipes are very efficient passive two-phase heat transport devices. Their high efficiency and low mass are desirable in the aerospace and electronics industries. The highly competitive nature of the thermal management industry results in little awareness of the capabilities of flat plate heat pipes, which has resulted in only a few applications of the technology. In the year 2000 a research and development project sponsored by Space Dynamics Laboratory was launched to investigate building carbon-based flat heat pipes. The flat configuration is desireable to incorporate many components onto one thermal management system. Development led to the adoption of the term "Channel Panel" because of the orthogonal grid of channels used as the capillary structure. Work to date has verified the utility and basic function of this technology but has not resulted in a standard method for the design and fabrication of channel panels. This study investigates and evaluates currently available and relevent models useful for the design of channel panels, investigates issues with fabrication, and makes suggestions for future development. Shallow pool

boiling is shown to be an appropriate model for the critical heat flux of boiling in flat plate heat pipes and provides a means for estimating the convective heat transfer coefficient. Previous work by Neal Hubbard is modified and shown to accurately couple the geometry and operating limits of a channel panel. Experiments verify the analytical predictions of these models. Issues in the fabrication of channel panels are reported as well as standard procedures for cleaning and filling. The final result is a standard method for the initial design phase of channel panel flat plate heat pipes.

(95 pages)

Much thanks to Andrew Decauster, Matt Sinfield, Blake Rusch, Devin Dalton, Kent Johnson and many helping hands at Space Dynamics Laboratory.

Acknowledgments

This work has been a great experience for all involved and it has been pleasantly executed due to the leadership of Drs. J.C. Batty, Leijun Li, and Scott Jensen.

James R. Harris

Contents

List of Tables

List of Figures

Chapter 1

Introduction

Heat pipes are highly effective heat transfer devices. They transfer heat through the evaporation and condensation of a working fluid. They are totally passive operating under their own internal pressure. There are two types of heat pipes cylindrical and flat. Cylindrical heat pipes have been used successfully for years in a variety of applications. They consist of a hollow pipe with hermetically sealed ends, a wicking structure on the interior surface and a working fluid. Flat heat pipes are the same except that their cross section is flat, usually rectangular. Flat plate heat pipes are potentially very useful for a variety of applications providing a versatile, low mass, high cefficiency device for thermal management. These advantages make flat heat pipes ideal for aerospace and high power electronics.

Space Dynamics Laboratory sponsored a research and development project in the Department of Mechanical Engineering in the year 2000 to investigate the possibility of building carbon based composite heat pipes in a flat plate configuration. The flat plate geometry was desirable for its ability to incorporate many components, including space radiators, into one thermal management system. Additionally, the increased area spread the heat, thus lowering the heat flux to manageable levels. The project has produced several prototypes and experimental results which show flat plate heat pipes may provide important new capabilities in thermal management systems.

The most important development has been the orthogonal grid of grooves or channels used as the capillary structure. This has led to the adoption of the term "channel panel." Though grooves have been used in heat pipes for years their advan-

tage in flat heat pipes, due to the two-dimensional geometry and close proximity to the heat source, is more pronounced. Liquid flows around obstacles in the grooves because of the open two-dimensional structure and they can be modified to include other capillary enhancements to improve performance.

In principle, cylindrical heat pipes and flat heat pipes differ only in their geometry. However, this creates many new problems for the engineer. Cylindrical heat pipes are generally used to transport a large quantity of heat from point to point. Flat heat pipes are intended to move heat from a high power density location to a low power density location. The vapor flow inside flat heat pipes is different than in cylindrical heat pipes and the higher interior surface area creates the need for more structural support. In order to design flat heat pipes the conventional equations for cylindrical heat pipes must be revised and new parameters investigated.

1.1 Conceptual Review

We will first begin with a review of the equations governing heat pipe operation [1, 2, 3, 4]. A review of subsequent literature indicates little has been done to improve upon the equations presented by these sources for the analytical evaluation of heat pipe operation limits.

The fundamental mechanisms in both cylindrical and flat heat pipes are similar. Heat added to an area evaporates the liquid into vapor which moves to the slightly lower vapor pressure associated with a cool area where the vapor condenses. The lower volume of liquid at the heat source creates a capillary pressure gradient in the channels that causes the recondensed liquid to flow back to the heat source to be evaporated again. The cycle will continue until any of several operating limits is reached. These are viscous, entrainment, sonic, boiling, and capillary limits.

Table 1.1: Nomenclature for Conceptual Review

T_{sat}(K)	Saturation temperature of the vapor	K_w	Friction coefficient of the capillary system
T_o(K)	Stagnation temperature of the vapor	A_w(m^2)	Cross sectional area of the capillary system
V_v(m/s)	Velocity of the vapor	ρ_l(kg/m^3)	Saturated liquid density
C_p(J/kg K)	Specific heat of the vapor	L_{eff}(m)	Effective length of the channels
ρ_o(kg/m^3)	Density of the vapor at the stagnation temperature	fRe_v	Coefficient for laminar flow of the vapor
ρ_v(kg/m^3)	Density of the vapor at the saturation temperature	fRe_l	Coefficient for laminar flow of the liquid
γ_v	Ratio of the specific heats of the vapor	μ_v(Pa s)	Vapor viscosity
A_v(m^2)	Cross sectional area of the vapor	μ_l(Pa s)	Liquid viscosity
λ(J/kg)	Latent heat of vaporization	C	Mach correction factor
R_v(J/kg-mol)	Ideal gas constant of the vapor	k_{ee}(W/m K)	Effective thermal conductivity of the capillary system in the evaporator
Q_s(W)	Sonic limit	k_l(W/m K)	Liquid thermal conductivity
ΔP_t(Pa)	Total pressure drop	k_{we}(W/m K)	Capillary system material thermal conductivity
ΔP_v(Pa)	Vapor pressure drop	ω(m)	Channel width
ΔP_l(Pa)	Liquid pressure drop	w_f(m)	Pedestal width
ΔP_{ah}(Pa)	Axial hydrostatic pressure drop	δ(m)	Channel depth
ΔP_{nh}(Pa)	Normal hydrostatic pressure drop	A_{wev}(m^2)	Surface are of the capillary system in the evaporator
ΔP_c(Pa)	Capillary pressure	R_{we}(K/W)	Thermal resistance of the capillary system in the evaporator
σ(N/m)	Surface tension	r_n(m)	Nucleation site radius
θ(rad or deg)	Contact angle	Q_b(W)	Boiling limit
r_c(m)	Capillary radius		
r_{hv}(m)	Hydraulic radius of the vapor space		

The viscous friction force reduces the vapor flow when the vapor pressure gradient is very small. The viscous limitation may be observed in long heat pipes where the vapor has to travel a long distance, that have very long condensers, that operate with cryogenic fluids, or when the panel operates below the design operating temperature and the fluid viscosity is high. In order to eliminate the problem the temperature can be raised or the working fluid can be changed usually for a fluid with a lower boiling point.

The viscous shear of the vapor on the liquid can overcome the surface tension or capillary pressure of the liquid. The vapor pushes the liquid back towards the

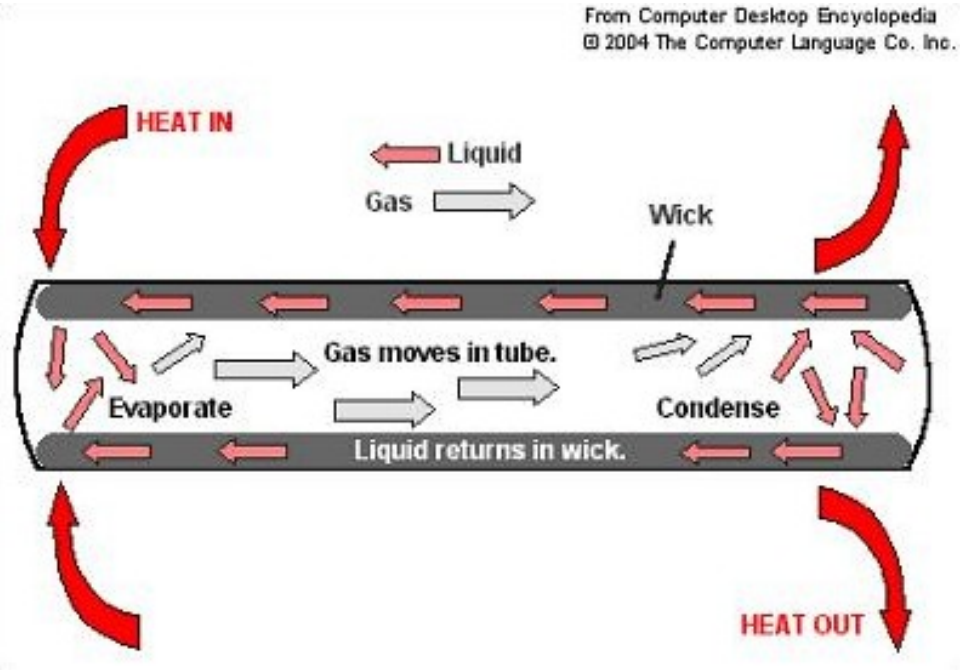

Fig. 1.1: Basic heat pipe operation. Reproduced with permission from Computer Desktop Encyclopedia (c) 1981-2008. The Computer Language Co. Inc., (www.computerlanguage.com).

condenser and may rip droplets off the surface, or entrain them, and carry them to the condenser. This can cause the condenser to flood and is known as the entrainment limit. This is caused by operating above the design power input or at too low an operating temperature. To prevent entrainment limitation requires an increase in the vapor space or operating temperature.

If the vapor velocity reaches Mach 1, the flow becomes choked. This usually occurs during start-up when the power input is high and the temperature is low. Because start-up conditions are transient, this problem usually corrects itself. A useful calculation for the design of heat pipes to prevent the sonic limit will be presented here.

If nucleate boiling occurs between the pipe wall and the wick, the vapor bubbles may impede heat conduction to the liquid film, and liquid flow into the evaporator.

High heat flux causes bubbles to form on the evaporator surface, resulting in dry-out, and high thermal resistances. A material with a higher heat flux capacity or better ability to spread the heat load will solve the problem.

When the pressure drop in the vapor, friction, and elevation head losses in the liquid flows are larger than the capillary pumping pressure in the wick, the mass flow rate out of the evaporator will be higher than the mass flow rate into the evaporator. Referred to as the capillary limit, this will cause dry out of the evaporator. The power input is higher than the design power transport capacity of the panel. To avoid this, capillary structure design must be modified or the power input reduced. Figure 1.2 and Figure 1.3 illustrate the relationship between the various operating limits. Each curve defines a set of temperatures and heat load (power in watts) that limit heat pipe operation. The area below each curve avoids the respective limit. The lowest limit is the characteristic limit of the heat pipe. Different heat pipes have different characteristic limits. As we can see by comparing Figure 1.2 and Figure 1.3, the lowest operating limit for Figure 1.2 is the capillary limit, and Figure 1.3 the lowest operating limit is the boiling limit. Four of these limits increase with increasing temperature and the boiling limit decreases with temperature increase. Together these limits define an operational envelope for the heat pipe.

Heat pipes are usually limited by the capillary or boiling limits. The other limits are usually avoided by an increase in temperature or a change in the geometry of the vapor space. For design, the capillary and boiling limits will provide guidelines for the geometry of the capillary structure, orientation of the heat pipe with respect to accelerations, the wall material thermal conductivity, and the maximum heat flux in the evaporator. The sonic limit is also useful because it provides a simple way to choose a appropriate cross-sectional flow area for the vapor space.

We have chosen to use channels because of the advantages gained by surface

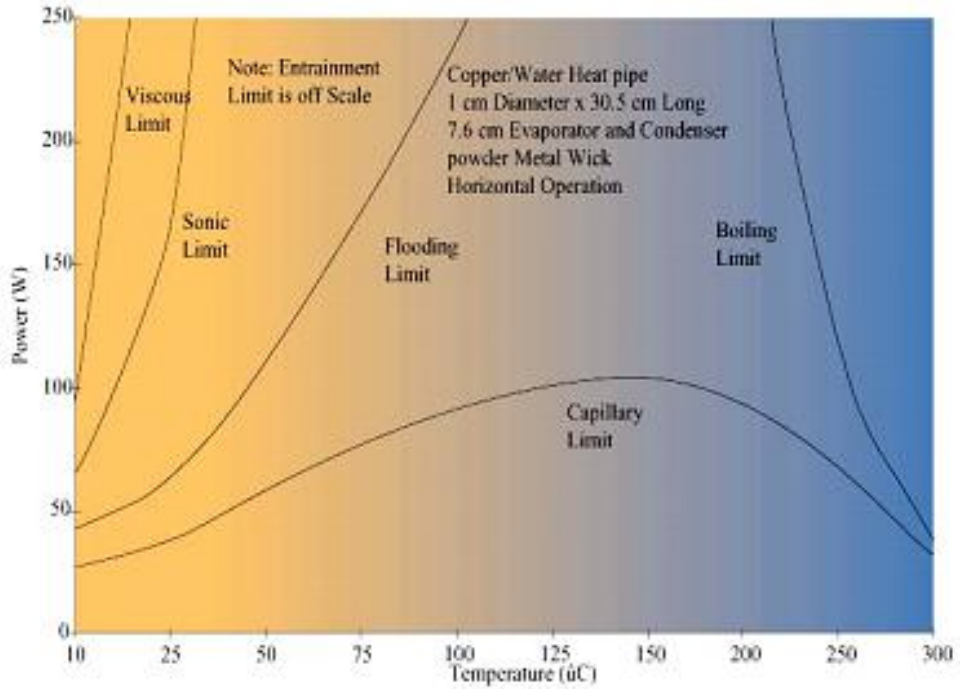

Fig. 1.2: Copper/water cylindrical heat pipe operating limits [5].

area, speed of the liquid, and wall thickness. The additional surface area reduces the heat flux in the evaporator. Axial, and lateral channels allow the liquid to travel through the wick in virtually any direction, thus potentially increasing the flow into the evaporator. More paths for the liquid to follow decrease the risk of drying out the evaporator. The channels are cut or built into the wall material which brings the heat source located on the external surface and the bottom of the channels where the phase change takes place, and the vapor space as close together as possible. This decreases the temperature change ΔT through the thickness of the panel walls.

1.1.1 Sonic Limit

Channel panel applications usually require that the panel have a small overall thickness. The thickness of the vapor space can account for one-third or more of

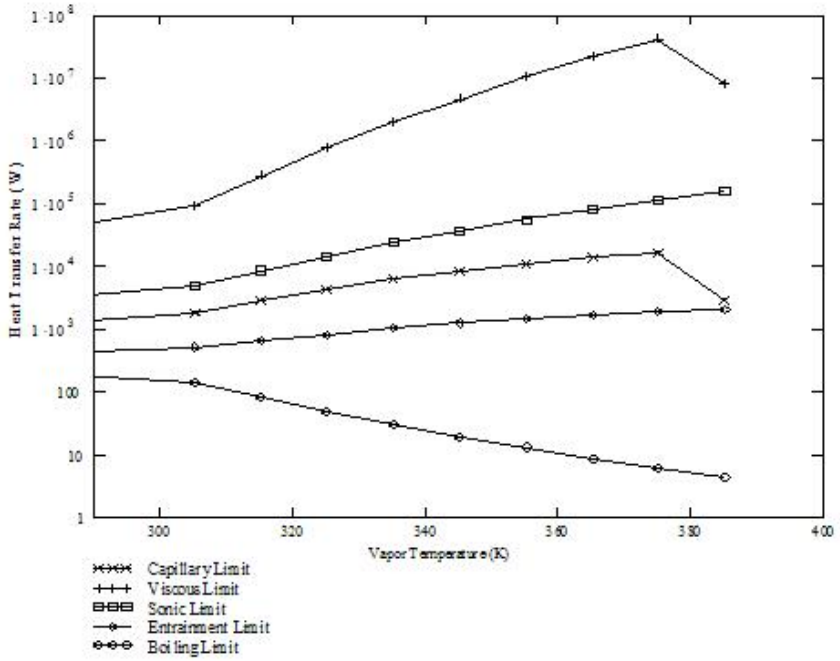

Fig. 1.3: Listed limits are predicted by the Hubbard Model [6] for a carbon composite axial grooved flat heat pipe.

the total thickness of the panel. The sonic limit is related to the cross-sectional area through which the vapor flows. To calculate the sonic limit we must have the stagnation temperature T_o, and density ρ_o of the vapor at various saturation temperatures. We calculate these using the vapor velocity, specific heat, vapor density, ratio of specific heats, and saturation temperature.

$$T_o = \left(T_{sat} + \frac{V_v^2}{2 \cdot C_p} \right) \tag{1.1}$$

$$\rho_o = \left[\rho_v \left(\frac{T_o}{T_{sat}} \right)^{\frac{1}{\gamma_v - 1}} \right] \tag{1.2}$$

The sonic limit is now calculated by Equation 1.3. The most important parameter is A_v, the cross-sectional area of the vapor space. If the area is too small the flow of vapor will reach Mach 1, which will choke the flow and cause high thermal gradients.

We will use this limit to design a vapor space to that minimizes compressible effects.

$$Q_s = \left[A_v \rho_v \lambda \left[\frac{\gamma_v R_v T_o}{2(\gamma_v + 1)} \right]^{\frac{1}{2}} \right] \tag{1.3}$$

1.1.2 Capillary Limit

The capillary pumping capacity of the wick is compared to the total pressure drop. If the capillary pressure is insufficient a smaller channel width or a different working fluid may be selected. The total pressure drop is calculated as the sum of the vapor, liquid, normal hydrostatic, and axial hydrostatic pressure drops.

$$\Delta P_T = \Delta P_v + \Delta P_l + \Delta P_{nh} + \Delta P_{ah} = \Delta P_c \tag{1.4}$$

The capillary pressure is calculated using the surface tension, and the capillary radius of the channels. Theta is the wetting angle of the fluid. This is a fluid-material interaction and will be different for every fluid, and wall material combination.

$$\Delta P_c = \frac{2\sigma \cos(\theta)}{r_c} \tag{1.5}$$

The capillary limit is calculated by adding or subtracting the hydrostatic effects depending upon where the evaporator is located compared to the condenser in gravity. For example, if the evaporator is below the condenser the hydrostatic head loss will assist the circulation of the fluid. The opposite is true, if the evaporator is above the condenser. The effective length L_{eff} is the distance from the evaporator to the leading edge of the condenser. The capillary structure cross-sectional area will be adjusted to improve the capillary pumping pressure. A reduction in the cross-sectional area of the vapor space will decrease the capillary limit because of increased friction loss

between the vapor and the walls of the vapor space. The Equation 1.6 calculates the capillary limit for a channel panel. Addition and/or subtraction of the different pressure drops would be changed for different orientations of the heat source with respect to the condenser in gravity.

$$Q_c = \frac{(\Delta P_c + \Delta P_{nh} - \Delta P_{ah})\,(2r_{hv}^2 A_v \rho_v \lambda K_w A_w \rho_l)}{L_{eff}\,(CfRe_v \mu_v K_w A_w \rho_l + 2\mu_l r_{hv}^2 A_v \rho_v)} \tag{1.6}$$

1.1.3 Boiling Limit

The boiling limit is found using a thermal impedance model for the wall and capillary system, and the area of the evaporator. First, we need to find the conductivity of the capillary system.

The simplest estimate for the conductivity of a groove capillary system is:

$$k_{ee1} = \frac{\omega k_l + w_f k_{we}}{\omega + w_f} \tag{1.7}$$

"This equation assumes that the [pedestals] transfer the same heat flux as the liquid. The actual heat transfer path is more complicated because evaporation only occurs at the liquid-vapor interface" [6]. With the effective thermal conductivity of the capillary system the thermal impedance of the evaporator is calculated by Equation 1.8. The area of the evaporator A_{wev} is the wetted surface area of the evaporator. This is different than the area of the heat source.

$$R_{we} = \frac{\delta}{k_{ee} A_{wev}} \tag{1.8}$$

Equation 1.9 [2] represents the boiling limit as a relationship between the pressure of a vapor bubble forming at a nucleation site and the capillary pressure of the channel.

Because the nucleation site radius is on the order of 10^{-7} meters, the pressure at the nucleation site dominates. After a fluid has been selected for the model, the thermal impedance R_{we} of the wall material in the evaporator will most affect the boiling limit. However, the latent heat, and the density can change the boiling limit by orders of magnitude if the saturation temperature is changed. Selection of the working fluid will be critical to the design. The boiling limit is a good tool for to choose wall material-fluid combination.

$$Q_b = \left[\frac{T_{sat}}{\lambda \rho_v R_{we}} \left(\frac{2\sigma}{r_n} - \Delta P_c \right) \right] \tag{1.9}$$

In summary, for the heat pipe to work properly according to design specifications, all equations need to be satisfied simultaneously for a range of operating conditions. However, a linear design rule that can be followed systematically by a designer is not currently available in open literature for flat plate heat pipes.

1.2 Literature Review

Recently, more research on flat heat pipes has become accessible in open literature. However, the volume of information directly addressing flat heat pipes still remains small. This is not the case for sources focusing on cylindrical systems [1, 2, 3, 4]. There is also a vast body of research available on the capillary motion and heat transport of fluids and two phase systems. The research presented in this section represents work directly applied to the flat plate heat pipes (FPHP). In each case a flat plate heat pipe has been fabricated and studied.

In a paper written by J. Esarte and M. Dominguez [7] several grooved FPHP's were tested and compared to a model. A Peltier device was used as the condenser. A prediction of the thermal resistance for a thermosiphon was $0.12\frac{K}{W}$ and was used

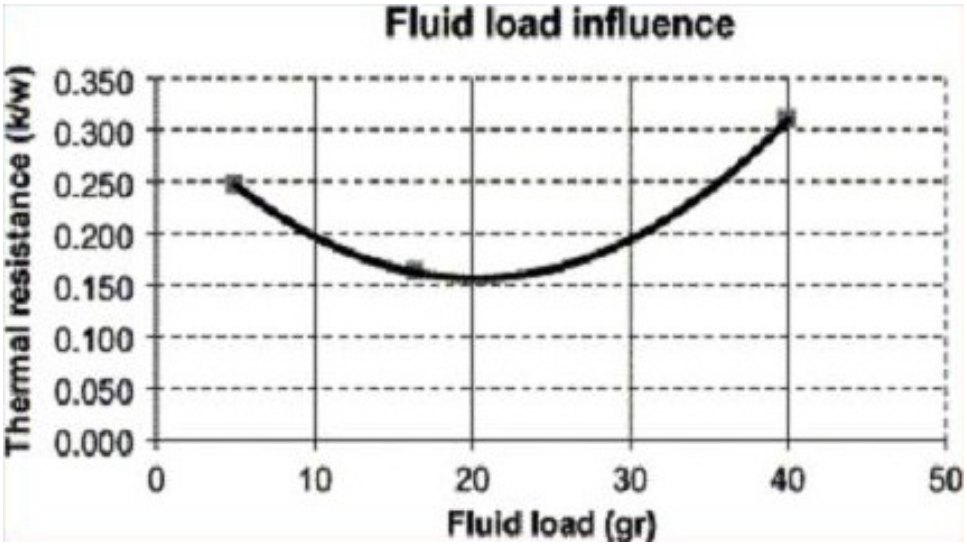

Fig. 1.4: Effect of fluid load on FPHP thermal resistance indicating an optimal charge volume [7].

to compare with the experimental results. How this prediction was made was not discussed. The working fluid was chosen based on a safety requirement to maintain the saturation pressure of the working fluid below atmospheric pressure. The figure of merit, and boiling regime were not considered. The initial efforts did not agree with the predicted values because no analysis seems to have been made on the capillary pumping pressure. Additionally, iterations of prototypes were made and tested based on observations from the first prototype. Several reasonable decisions were discussed as to what changes would be affected in the subsequent prototype but no mathematical approach was mentioned. Finally, the effect of fluid load (charge volume) on the thermal resistance of the FPHP was briefly examined. No criteria were mentioned for choosing the charge volume for a particular range of heat fluxes.

Avenas studied the possibility of using flat heat pipes as thermal spreaders for Insulated Gate Bipolar Transistors (IGBT) [8]. The simulation was performed using the Flowtherm software that uses a finite volume method and each medium in the heat path was given an equivalent conductivity. These were: the wall material, evaporator

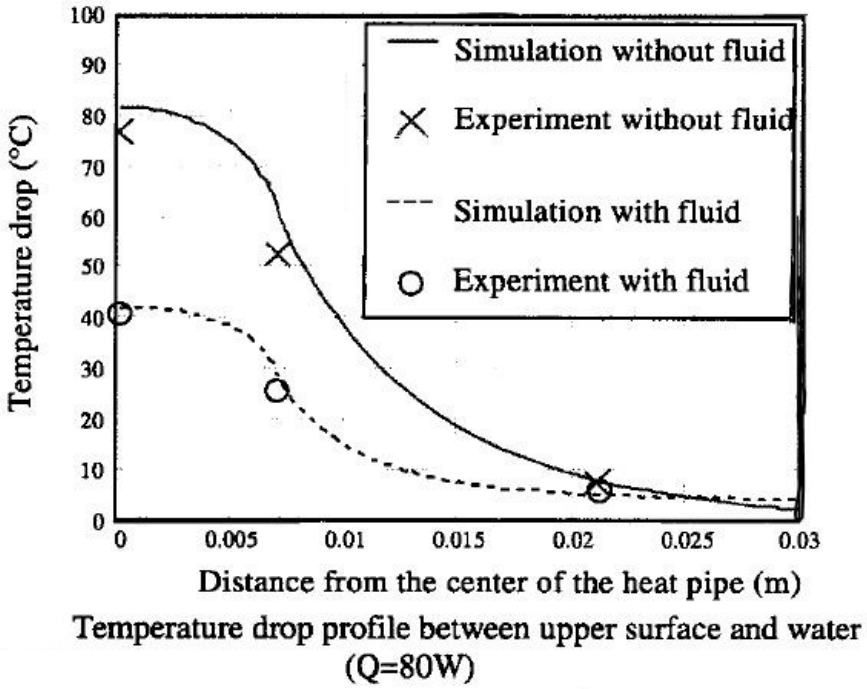

Fig. 1.5: Figure showing the correlation between numerical model and experiment [8].

wick, condenser wick and the saturated vapor space. Sintered powder wick and rectangular groove wick flat heat pipes were studied analytically in comparison to a plain copper or plain silicon sink. Finally, experimental data were compared to the model predictions. The data showed good agreement between the simulation and the experimental results. See Figure 1.5. However, nothing was discussed as to how the vapor space, the wick structure, the working fluid, and operating temperature were chosen.

Dr. Harder of curamik® electronics published a very interesting experimental study of a small flat heat pipe 80 x 30 x 3 mm [9]. The objective of this experimental investigation was to design and build a FPHP to meet specific operational requirements. These requirements were met and exceeded. One of these requirements was to reduce the thermal resistance of the pipe so that the effective conductivity was at

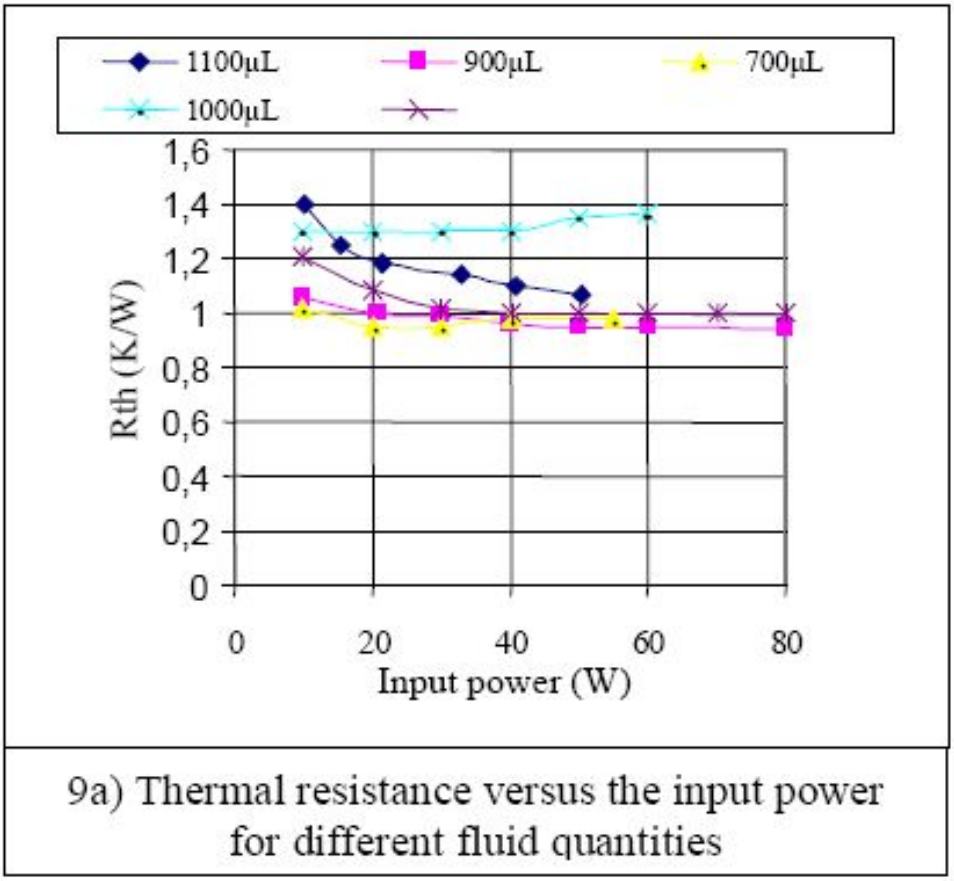

Fig. 1.6: Thermal resistance figure from Harder [9].

lease 5 times that of aluminum. Several charge volumes were used and the thermal resistance for various power settings reported. Figure 1.6 shows the thermal resistance of the FPHP was reduced for different charge volumes. This could mean there is an optimal charge volume where the thermal resistance is decreased at low power input.

This FPHP was capable of spreading $100W$ at a heat flux of $76\frac{W}{cm^2}$, for longer than three months without any loss in functionality. The FPHP was fabricated with a copper mesh wick, copper wall material, and the working fluid was either water or alcohol. Various cycles of heating did not affect functionality. The requirements for the heat pipe size and operation were reported together with the actual size and

Table 1.2: Design Objectives and Achievements [9]

	Specification or criteria targeted	Status of achievement	
Mechanical	Heat pipe size: 80 x 30 x 3mm	Manufactured	✓
	Thickness: 2mm	2.4 to 3mm	✓
	Mass: 35grams maximum	31 to 33grams	✓
Thermal performance	Dissipation up to 30W	Dissipation limit around 100W	✓
	Hot spots: 15W/cm^2	Limit power density around 76W/cm^2	✓
	At least 5 times the thermal conductivity of aluminium (>750W/m°C)	$\lambda_{heat\ pipe} \approx$ 900W/m°C (R_{th}=1°C/W– L=80mm-S=3mm x 30mm)	✓
	No deviation of thermal properties in horizontal/vertical position	OK	✓
Operational performance	Thermo-mechanical stress cycles (-55/+125°C) in vacuum	OK after 20 cycles	✓
	Operating and cold starting	OK after 4 cycles	✓
	Burst pressure (9.28bar) or proof pressure (4.64bar)	OK	✓
	No leakage	OK after 3 months	✓
	Mechanical tests	Not carried out yet	⊖

operation limits, see Figure 1.2. However, no information was provided as to why one or the other working fluids were chosen, or how design decisions were made for the choice of the wick structure and other parameters. This was an experimental study and no models were used.

The upper limits of the pipe were tested for the effect of charge volume on the pipe operating temperature. When charging a heat pipe the total volume of working fluid placed inside the pipe must create vapor-liquid equilibrium at a quality greater than the critical point. If too little fluid is used then the wick is not fully saturated and the wick will dry out resulting in failure of the pipe. The former is not difficult to achieve, however, the latter requires understanding of the thermal resistance through the wick. For the purposes of design it is needful to know what range of charge volume is best.

Y. Wang and K. Vafai have each written several papers on FPHP's [10, 11, 12, 13].

They have produced experimental, analytical, and numerical results which describe the performance of flat heat pipes. The focus of their efforts has been to compare the analytical model to empirical data. Therefore, they have become an important source for basic equations, and qualitative concerns for FPHP's. All four of the above mentioned papers are for an asymmetrical flat plate heat pipe. The first, [10], produces a pseudo-three-dimensional model for steady incompressible vapor, and liquid flow. This paper represents the some of the first efforts to predict the operating characteristics of a FPHP. The results of their investigation are used repeatedly in later works.

Their most recent [13] uses a conduction model to predict the maximum surface temperature for various heat fluxes. The objective for this latest was to introduce a time constant for the transient characteristics of a FPHP. In their paper a good agreement between the experimental and analytical data was achieved, see Figure 1.7. The analytical data for this figure was produced using a conduction model. This model is not completely described in the paper but takes into account the "room temperature, input heat flux, the heat transfer coefficient [off the condenser surface into the room], and the thermophysical and geometric parameters of the heat pipe..." [13]. Therefore, simplified models can be used to accurately predict the overall operation of FPHP's, when used together with an accurate prediction of the internal fluid-thermodynamic mechanisms.

Y. Wang and G. P. Peterson [14] experimented with a small FPHP with dimensions 152 x 25 x 2.7 mm. The thin walls, only .254 mm thick, were supported by axially oriented wires that separated the walls from each other, and a screen wick was used between the walls and the wires, see Figure 1.3. Analysis was performed to predict the various operation limits. The operating limits were predicted using equations previously identified in Peterson's Book on heat pipes [2].

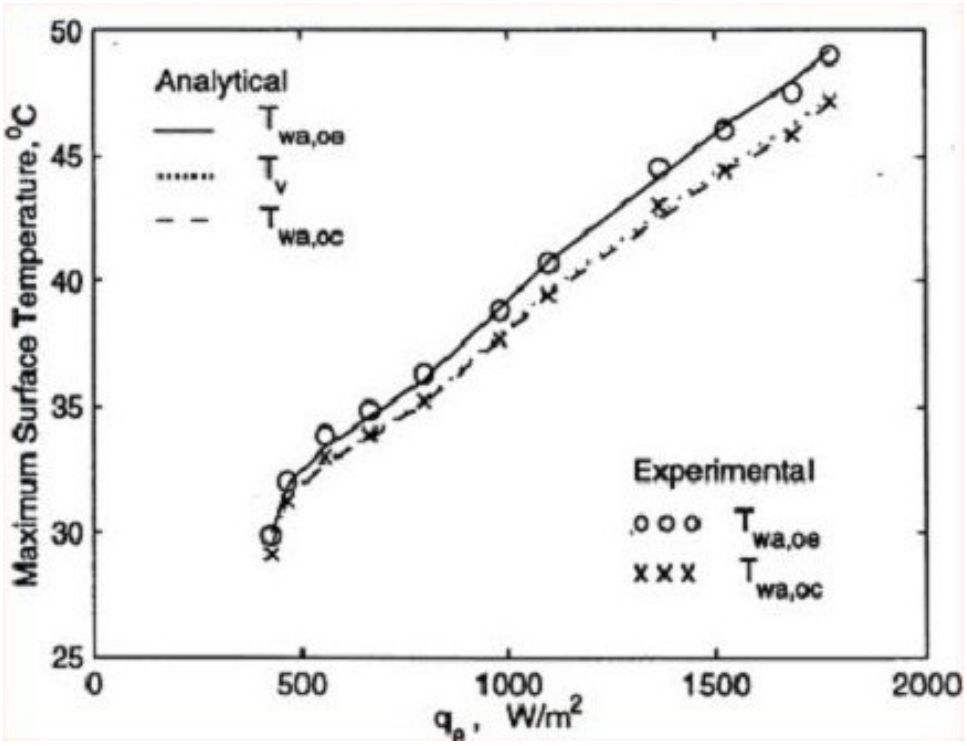

Fig. 1.7: Effect of the heat flux on the maximum surface temperature [13].

They report that the maximum heat transport capacity was affected by the mesh number, wire diameter (vapor space thickness), wick thickness, orientation and length. The mesh number and length have a less significant effect on Q_{max}while the size of the vapor space, wick thickness and orientation all strongly affect Q_{max}. Figure 1.8 shows the correlation between the model and the experimental results were good. However, the needs of a consumer were not addressed. Rather their works focused on the ability to model and predict heat pipe operating limits of an existing prototype. This is useful when a design exists to be evaluated. But an analytical systematic determination of the design is needed so that the cost of building many prototypes can be avoided.

M. Cerza and B. Boughey investigated the effect of air infiltration on the temperature profile of a large flat heat pipe measuring 1.22 x .305 x .0127 m [15]. The

Table 1.3: Physical Specification of the Flat Heat Pipes [14]

Flat heat pipe	Prototype 1	Prototype 2
L, mm	152.4	152.4
L_e, mm	25.4	25.4
L_c, mm	50.8	50.8
t_w, mm	0.254	0.254
Wick structure	#100 screen	#150 screen
Layers	4	6
d_s, mm	0.813	0.813
S_w, mm	2.5	2.5
H_p, mm	2.71	2.52

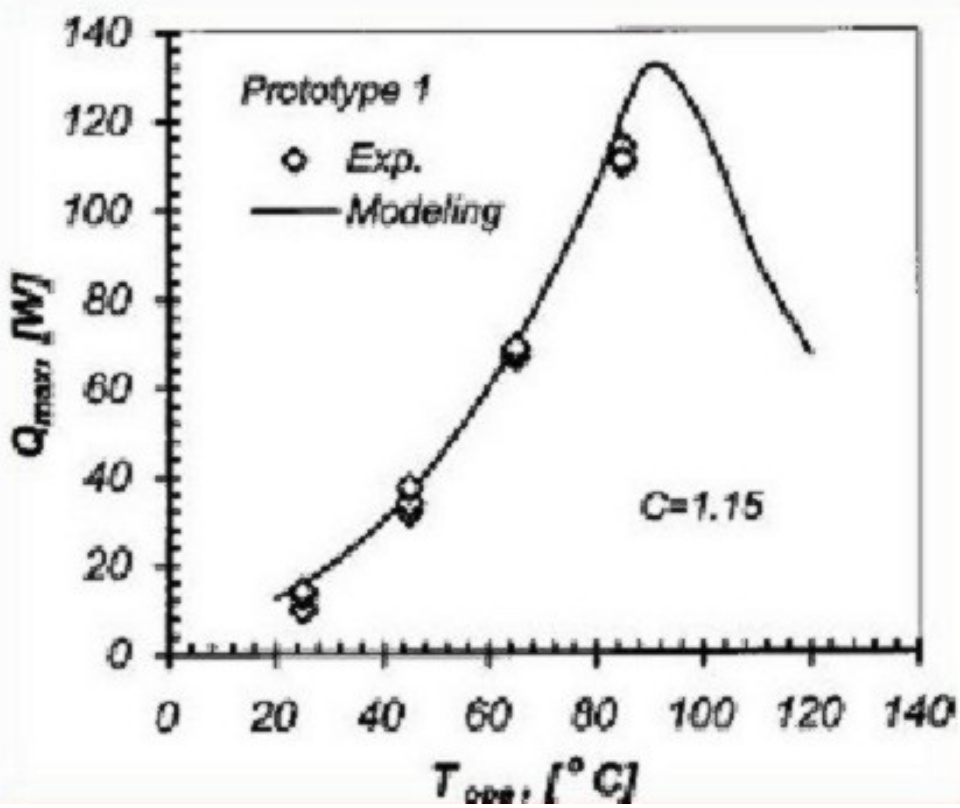

Fig. 1.8: A comparison of the experimental and modeling results of the Prototype 1 flat heat pipe [14].

h	Convective heat transfer coefficient	R_g	Gas constant
C	Condenser perimeter	R_v	Gas constant of vapor
L_c	Condenser length	T_o	Referance operating temperature
h_{fg}	Latent heat of vaporization	T_{amb}	Ambient temperature
m	non-condensable mass	T_g	Temperature of gas in the inactive condenser region
P_o	Reference operating pressure	T_v	Temperature of vapor in the active condenser region
P_{vi}	Vapor pressure of fluid in the inactive condenser end	A_v	Vapor core cross sectional area
Q	Heat input		

Fig. 1.9: Nomenclature for Cerza [15].

pipe was compared to a type of cylindrical heat pipe which has a gas reservoir in the condenser, and is called a variable conductance heat pipe. An infrared camera was used to visualize the interaction of the air and working fluid inside the pipe. Cerza used a correlation by Marcus and Fleishman [16] for the prediction of the heat transport in a variable conductance heat pipe without a gas reservoir. This is given in Equation 1.10 and the nomenclature in Figure 1.9.

$$Q = hC\left(T_v - T_{amb}\right)\left[L_c - \frac{mR_gT_g}{\left[P_o \exp\left(\frac{h_{fg}}{R_v}\left(\frac{1}{T_o} - \frac{1}{T_v}\right)\right) - P_{vi}\right]A_v}\right] \tag{1.10}$$

The results showed a strong effect on how much of the condenser was blocked by a non-condensable gas (air) when the pipe was operating horizontally. They reported minimal effect for the vertical orientation. The qualitative results of this investigation illustrate the importance of preventing leaks in a FPHP. However, as shown in Figure 1.10 and 1.11, the correlation between the analytical and experimental results was not consistent. Cerza discussed this inaccuracy, but the results demonstrate that it would be difficult to have confidence in a prediction of some allowable volume of non-condensable gas using the cited theory.

Cerza addressed an important concern in all heat pipes, contamination. His study was performed on a large flat plate heat pipe and only considers the effect

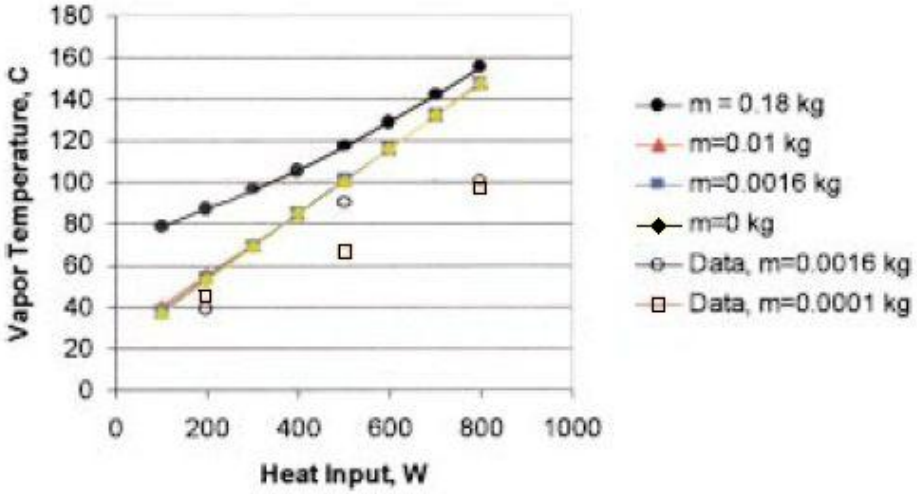

Fig. 1.10: Comparison of data to flat profile theory 1 [15].

of air infiltration on the active condenser length of the heat pipe. The ratio of the volume of contaminant to the volume of the vapor space is not studied. This leaves some question as to how adverse the effects would be for small flat heat pipes vs. large flat heat pipes. As with other papers his work was primarily focused on a single prototype and did not suggest how to design a FPHP.

A dissertation written by Chuanbao Gu in 1995, investigated shallow pool boiling and elements of flat plate heat pipes (FPHP) [17]. The several chapters cover heat transfer limits of FPHP's, critical heat flux of shallow pool boiling, vaporization heat transfer of various surfaces, and the thermal performance of a FPHP. The relationship between critical heat flux and vaporization heat transfer of different surfaces in shallow pool boiling is central to understanding the FPHP boiling limit, and to determine the boundaries of the boiling curve. Gu reviews the four mechanisms postulated since 1948 explaining the critical heat flux in pool boiling and carefully points out their weaknesses and strengths. The focus of his review lies mainly on the hydrodynamic instability model proposed by Zuber in 1959 and the macrolayer

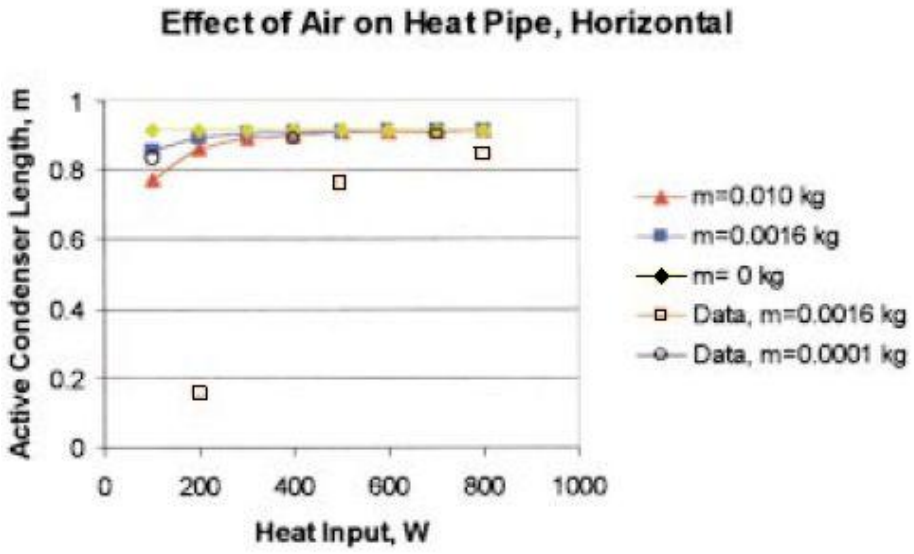

Fig. 1.11: Comparison of data to flat profile theory 2 [15].

dry-out model proposed by Haramura and Katto in 1983. The following quote from Gu's paper explains how the Zuber equation is insufficient for FPHP's.

> Initial criticism of Zuber's CHF model, as reflected in the works of Bernath (1959), Costello and Frea (1963), and Chang (1963), centered on the fact that the CHF model did not account for possible effects of the geometry, surface condition, and wetting characteristics of the heater surface. Experimental data available at that time suggested that these factors could significantly affect the CHF condition.[17, pp. 67]

These are important issues because the surface geometry, condition and wetting characteristics are chosen specifically to enhance both the heat transfer coefficient and the CHF in channel panels. One of the features of the macrolayer dry-out model is that "a thin liquid sublayer adjacent to the surface that is replenished only after the large bubble covering it departs" [17]. Gu criticizes this point based on experimental observations where vapor bubbles were separated from the liquid sublayer by vapor

jets, which suggests that the liquid was replenished before the bubble covering that surface departed. The strength of the macrolayer model is that it is the only model which can include many secondary effects such as heater geometry, surface condition, and wetting. Later in his study Gu uses the macrolayer dry-out concept to analyze the critical heat flux for shallow pool boiling.

The details for the experimental setup to test the Macrolayer dry-out model can be found in chapter 4.3 of Gu's paper. Several boiling curves were generated for different heights of liquid above the circular heated plate for the liquid FC-72. The prediction for the CHF using the macrolayer dry-out Equations 1.11 and 1.12 are shown below. Comparing these to the boiling curves in Figure 1.12 and Figure 1.13 it is obvious that the macrolayer dry-out prediction matches the CHF results but only if the liquid level is above some critical value which for this liquid is ~12.0 mm. This means that the macrolayer dry-out model is not appropriate if the liquid level is below the critical height H_c. The implication is that these models should not be used for any FPHP where the liquid level is below H_c.

$$q_{z,c} = 0.131 \rho_v h_{lv} \left[\frac{\sigma \left(\rho_l - \rho_v \right) g}{\rho_v^2} \right]^{\frac{1}{4}} = 14.1 \cdot 10^4 \frac{W}{m^2} \tag{1.11}$$

$$\frac{q_c}{q_{z,c}} = (1+k)^{\frac{5}{16}} \left[48\pi \frac{\sigma}{g \left(\rho_l - \rho_v \right)} \frac{1}{D^2} \right]^{\frac{1}{16}} = 1.17 \tag{1.12}$$

$$q_c = 16.5 \cdot 10^4 \tfrac{W}{m^2}$$

Gu continues by deriving an expression for H_c, Equation 1.13, based on the pressure difference between the liquid surrounding the bubble and the liquid at the heated surface. Details of the derivation can be found on pages 107-110 of Gu's paper

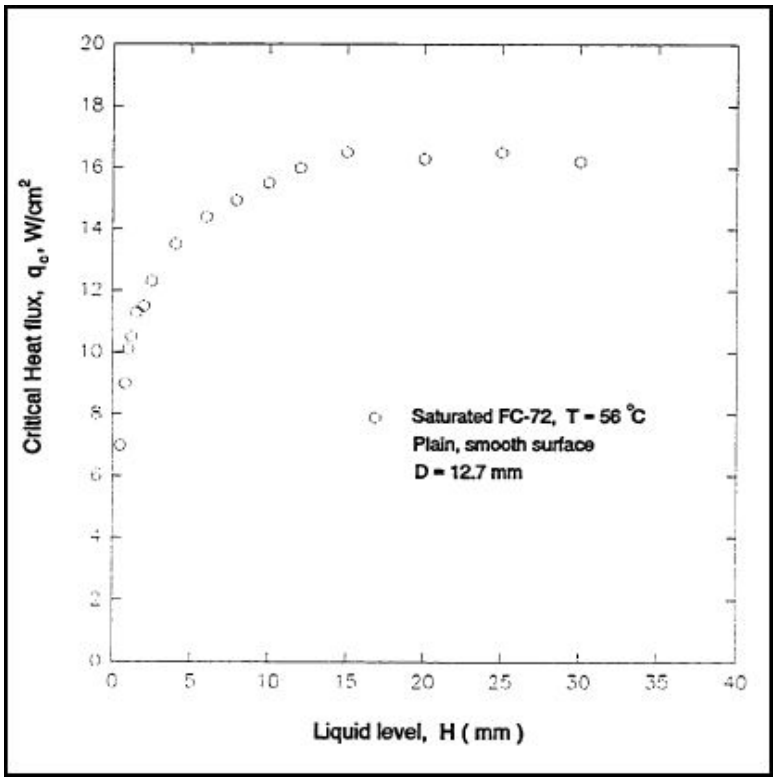

Fig. 1.12: Effect of liquid level on CHF for FC-72 [17].

resulting in the following equation. The experimental and analytical results agree very well though as Gu suggests more liquids should be tested.

$$\frac{H_c}{D} = 1.252 \left(\frac{q_c}{g^{\frac{1}{2}} D^{\frac{1}{2}} \rho_v h_{lv}} \right)^{\frac{2}{5}} \tag{1.13}$$

Gu derives Equation 1.14 for the CHF for any height of liquid. Equation 1.14, relates the macrolayer dry-out CHF q_c to the constant ϕ which, must be determined experimentally for different liquids, and the height H. In Figure 1.14 the experimental results agree closely with the prediction except below a liquid height of $1mm$. ρ_v and ρ_l are the vapor and liquid densities respectively, σ is the surface tension, D is the diameter of the heated area, g is gravity, and h_{lv} is the heat of vaporization.

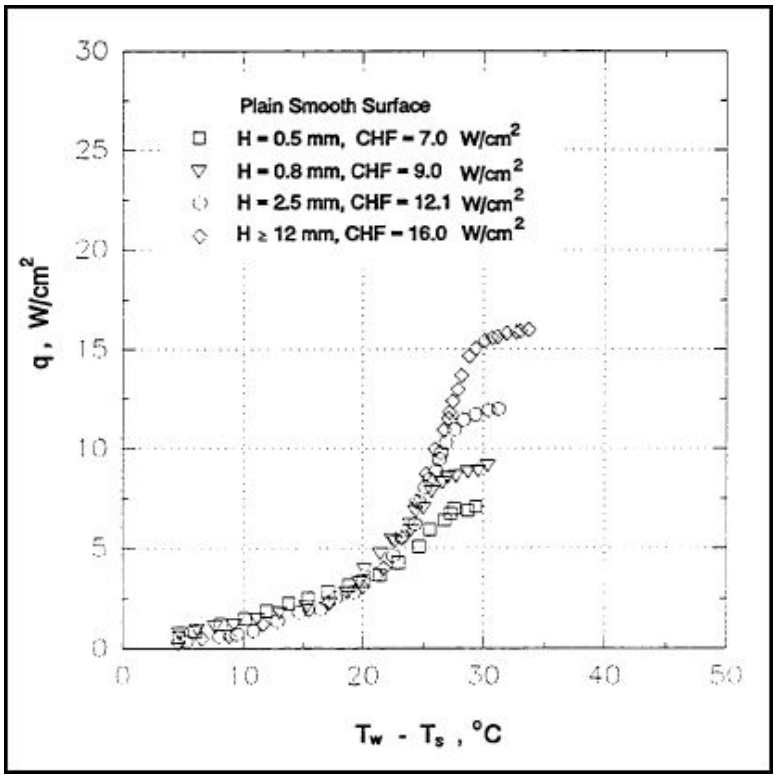

Fig. 1.13: Boiling curves of a plain flat surface with different liquid levels as presented by Gu [17].

$$\frac{q_c}{\rho_v h_{lv}} = 1.289\phi \left(\frac{\rho_v}{\rho_l}\right)^{\frac{2}{15}} \left[\frac{\sigma\rho_l}{\rho_v^2 D}\sqrt{2gH}\right]^{\frac{1}{3}} \tag{1.14}$$

Gu performs three groups of experiments to find the CHF for a given height of fluid under various surface conditions to show the effect of surface geometry on CHF. These three groups of experiments are:

- flat surfaces covered with a screen mesh of varying mesh number (ch. 5)
- Microstud and microgroove surfaces covered, and uncovered by a screen mesh of varying mesh number (ch. 6)

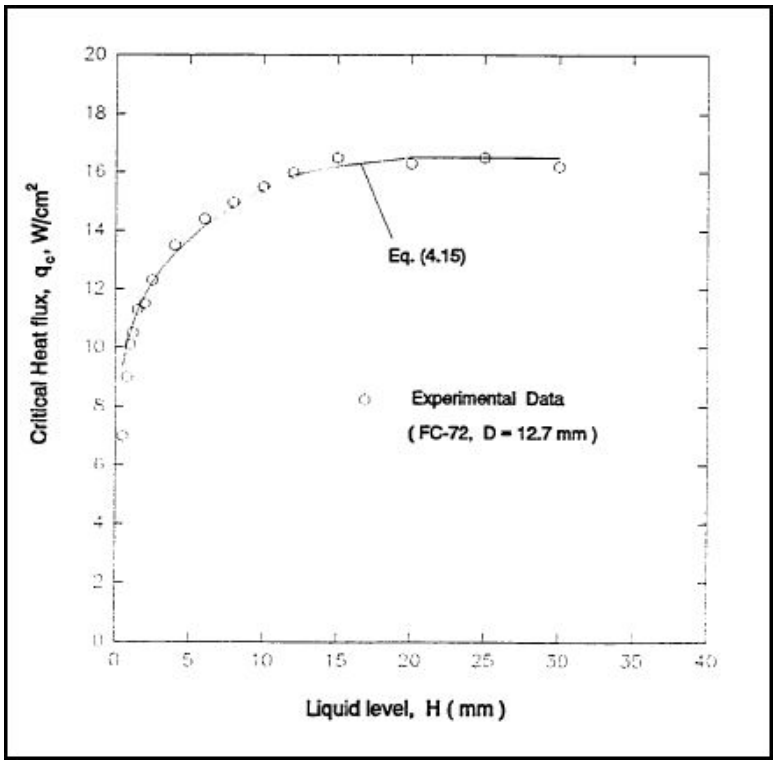

Fig. 1.14: Correlation of experimental and analytical results [17].

- Flat plate heat pipe using a flat surface covered by a screen mesh (ch. 7)

The data in Figure 1.15 are taken from chapter 5 and chapter 7 respectively. They show good agreement between the plain flat surface covered by a screen mesh and the FPHP plain flat surface covered by the same screen mesh. Additionally, Gu observed that the CHF is virtually unaffected by liquid height when the surface is covered by a screen mesh of a sufficiently high mesh number.

Chapter 6 in Gu's paper is a collection of experiments detailing the effect of liquid height and surface geometry on CHF and "boiling incipience" also referred to as the "onset of nucleate boiling." A microstud or microgroove surface is a surface of posts or directional grooves similar to channel panels but without any specific pattern and not necessarily oriented to provide a direct liquid path from the condenser to the evaporator. Several figures clearly indicate that the CHF for a microstud or

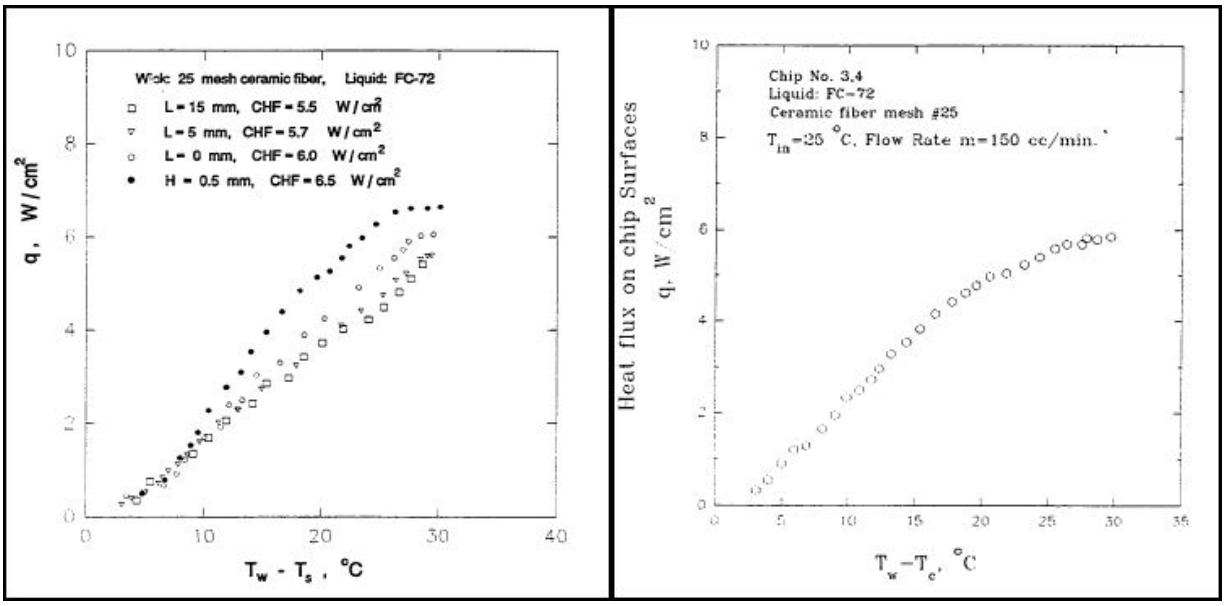

Fig. 1.15: Comparison of CHF of a flat surface with a #25 ceramic mesh (left) to a FPHP with a #25 ceramic mesh wick (right) [17].

microgroove surface uncovered by a screen mesh is greater than a flat surface or a rough surface at any given liquid height H. Indeed, the CHF for a microstud or microgroove surface is greatly increased over the CHF for a flat surface and liquid height above H_c! Referring to the table in Figure 1.16 Gu reports that for a liquid height of 2mm with a microstud surface the CHF is the same as for a plain flat surface at 12mm. The following statements are conclusions for shallow pool boiling.

1. The Zuber equation and Macrolayer dry-out model are insufficient for shallow pool boiling if the liquid height is below H_c and the analysis of boiling in FPHP's generally involves liquid heights below H_c.

2. The CHF prediction of Equation 1.14 closely agrees with the experimental results for a plain flat surface.

3. The plain flat surface covered by a screen mesh produces the same CHF as a FPHP plain flat surface covered by a mesh of the same mesh number. This

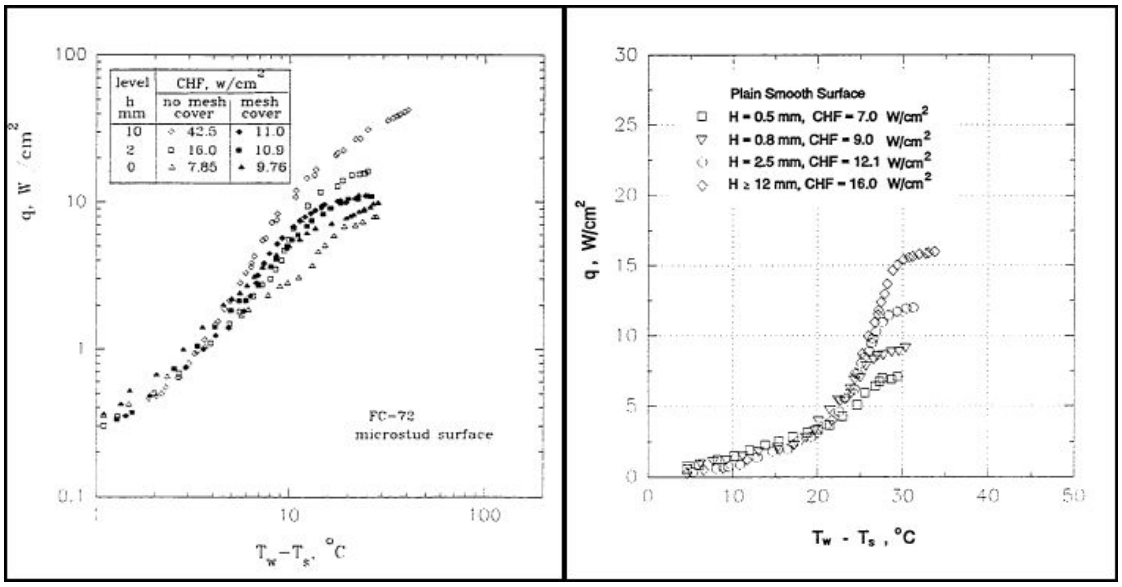

Fig. 1.16: Comparison of CHF of a microstud surface to a plain flat surface [17].

means that boiling in FPHP can be analyzed as a semi-infinite plate.

4. Channel panels increase the CHF limit and decrease the onset of nucleate boiling which results in a larger heat transfer coefficient at lower excess temperatures because channel panels use studs and grooves as the surface geometry.

5. From a knowledge of H_c and q_c a charge volume can be chosen to maximize the CHF and/or heat transfer coefficient.

6. From H_c and q_c the boiling heat transfer coefficient h_{boil} can be obtained.

1.3 Objectives

In order to provide the necessary design tools in my study I will:

- Evaluate current available and relevant models for the boiling limit, capillary limit, and the vapor flow.

- Develop appropriate predictive correlations useful for FPHP design.
- Address material-working fluid compatibility issues.
- Design a working prototype based on predictive models which will be fabricated using resources provided by Utah Center for Excellence in Thermal Management Technologies.
- Explore issues with welding, gluing, soldering, joining and sealing FPHP's.
- Test performance of the channel panel prototype, evaluate test data and compare with predicted results.

Chapter 2

Modeling and Testing

2.1 Effect of Fluid Level in Channels on Capillary Pumping Pressure

We discussed in 1.1.2 that the capillary pressure is related to three parameters. Surface tension, channel width, and wetting angle that depends upon the liquid-material combination. We will focus on the first two parameters. For surface tension in the liquid, the transformation pressure, and temperature of a liquid with a flat surface is different than those of a liquid with a curved surface. The change in pressure or temperature is written as ΔP and ΔT, respectively. These are not gradients in the fluid column but are deviations in the transformation pressure, and temperature from that of a flat surface. This is caused by the presence of a curved surface [18]. The following equation is derived by Brian Williams [18] from the laws of thermodynamics and Gibbs function.

$$(\nu_v - \nu_l)\,\Delta P + \nu_l \sigma C + (s_l - s_v)\,\Delta T = 0 \tag{2.1}$$

Where ν_v is the specific volume of the vapor phase, ν_l is the specific volume of the liquid phase, s is entropy, C is the curvature of the meniscus, and σ is the surface tension. Curvature is positive for a convex surface and negative for a concave surface. If the fluid surrounds a vapor bubble the surface is convex. The following is the equation for curvature. We immediately recognize that r is the channel width from the capillary pressure equation.

$$\pm C = \frac{2}{r} = \frac{4}{d} \tag{2.2}$$

We will consider the simple case of constant temperature. We will not consider the constant pressure case because channel panels operate by pressure gradients. The resulting pressure, based on Equation 2.1, of the fluid in the meniscus P_c varies by:

$$\Delta P = \sigma C \left(\frac{\rho_v}{\rho_v - \rho_l} \right) \tag{2.3}$$

where ρ_v is the density of the vapor phase and ρ_l is the density of the liquid phase, where ΔP is negative if the curvature is positive.

$$P_c = P_{flat} - \Delta P \tag{2.4}$$

In Equation 2.3 the liquid density is greater than the vapor density, the denominator will be negative. Positive curvature will decrease P_c and negative curvature will increase P_c according to Equation 2.4. In channels the curvature is negative unless bubbles are present. The fluid in the meniscus will evaporate at a slightly lower pressure than the plane surface. This will increase the mass flow of the vapor from liquid-vapor interface rather than between the wall and the liquid only. The combination of pressure drop and mass flow cause the liquid in the channels to flow toward the evaporator. A decrease in the channel width, r, will increase the curvature which is negative for a panel operating below the boiling limit.

My observation was that the curvature would also change in a channel if the channel was too full or too empty. The surface tension will pull the liquid up and over the edge of the channel walls if the fluid level is too close to the top of the channel. The fluid will attempt to level itself. This decreases curvature and the mass flow rate of vapor from the meniscus. Brandt [19] has a similar Figure 2.2.

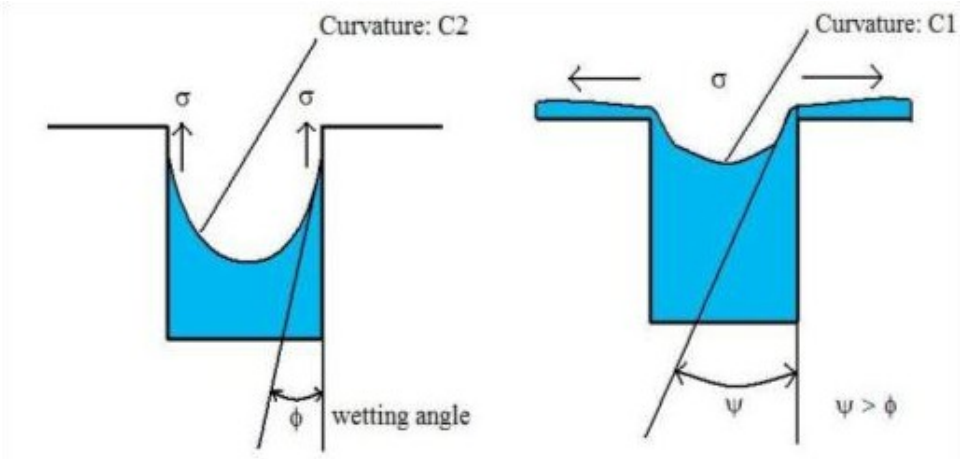

Fig. 2.1: Effect of liquid height on curvature.

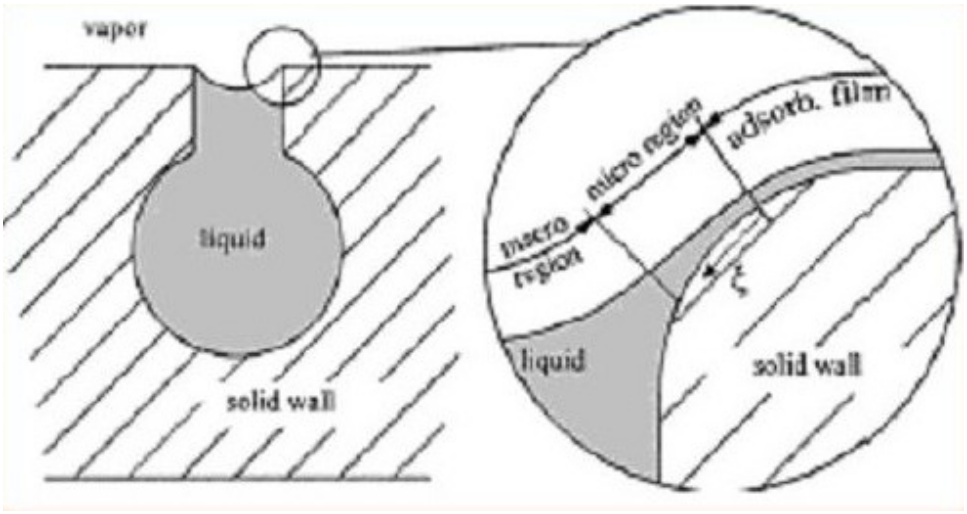

Fig. 2.2: Meniscus extending around a corner in a capillary groove [19].

2.1.1 Investigation

We decided to investigate fluid level this effect experimentally to see if it would be significant. Using a Santa Barbara Focalplane SBF-119 IR camera we recorded the temperature gradient of the entire panel and compared the data with visual

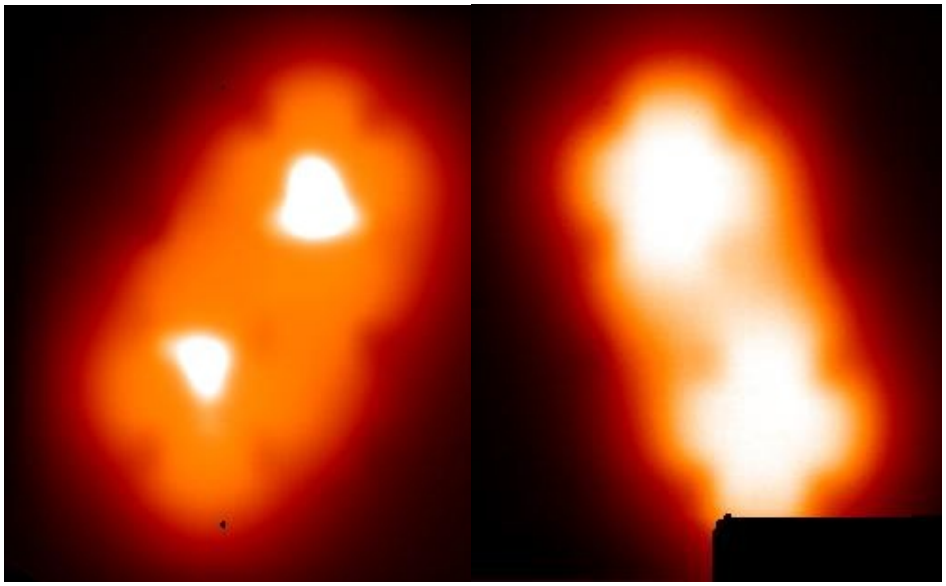

Fig. 2.3: 10 and 15% full respectively; Bright region is higher in temperature.

observations made possible by the transparency of the polycarbonate material. We changed only the volume of fluid used to fill the channel panel. This was calculated to be some percentage of the total volume of the channels both top and bottom, and excludes the vapor space entirely for this part of my study. The volumes tested were 10, 15, 20, 30 and 50%. Since the channels in this panel were large and the panel was placed horizontal gravity would force most of the fluid into the bottom and thus double, approximately, the amount of fluid in the channels on the bottom of the panel. The evaporator was set to $10W$ and the condenser was the top surface of the panel exposed to air in free convection at $20°C$.

In Figure 2.3 only the length and width of the panel is shown, dry spots are clearly visible for the 10% full test on the left where the bright areas were at a higher temperature than the bright areas for the 15% full test on the right. Not visible to the IR camera for the 15% test the dry spots were observed visually during the test. This means we are nearing a value which will not dry out at this power input. In Figure 2.4 and all similar figures, the lines are temperature data taken from virtical

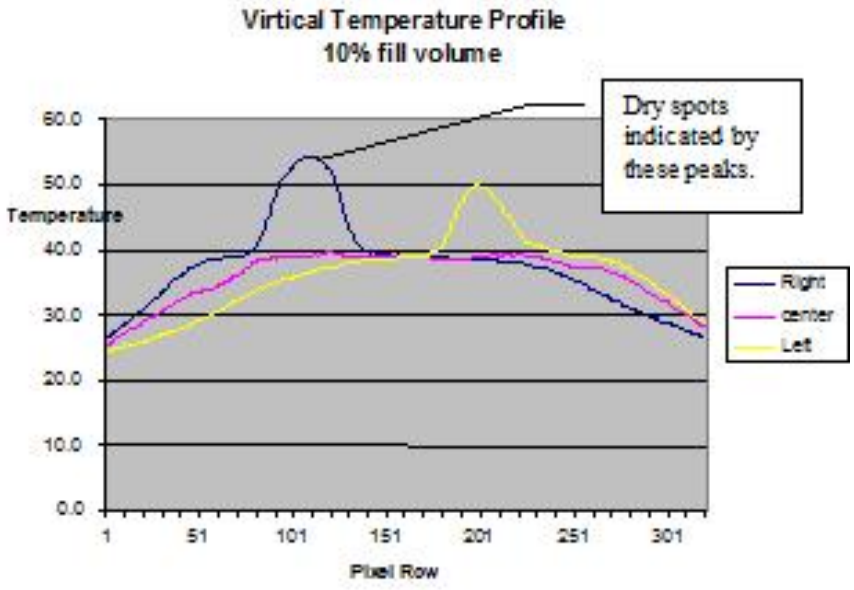

Fig. 2.4: 10% fill temperature vs. location; Each line is a virtical column of temperatures recorded by each pixel.

lines of pixels in the IR camera, and "virtical" means through the length of the IR camera image shown. The camera numbers the pixels beginning at zero top to bottom. The computational error in coverting from camera units to temperature is $T^{+2°C}_{-0.0°C}$.

Test with 50% full fluid photo was taken at an angle but we can see that the panel is performing similar to the 30% test on the left. There are no dry spots, and the temperature is more uniform than the 10 and 15% tests. Note in the following graphs the wavy condition of the curves are where the dark spots are seen in the photos, which are structural supports inside the panel.

The tests at 10 and 15% were observed to produce a dry evaporator and/or a small isothermal zone, and I observed that the temperature of the heaters was higher for the 10 and 15% tests because there was too little fluid to maintain wetting in the evaporator. The panel was unable to dissipate the heat and so the excess heat was dissipated through the insulation which was plastic foam and was slightly melted. The IR camera recorded a profile which was peaked rather than a flat plateau

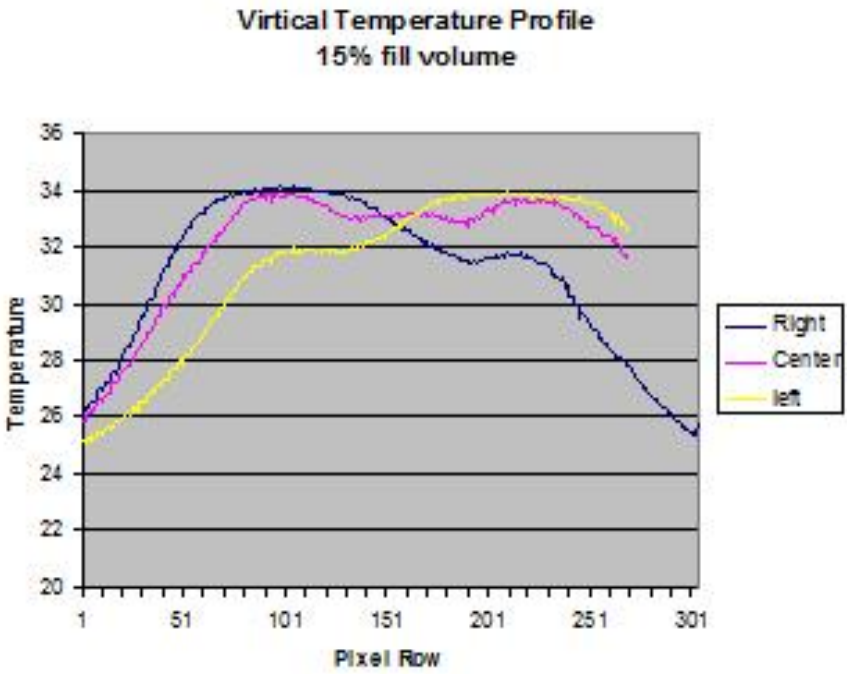

Fig. 2.5: 15% fill temperature profile.

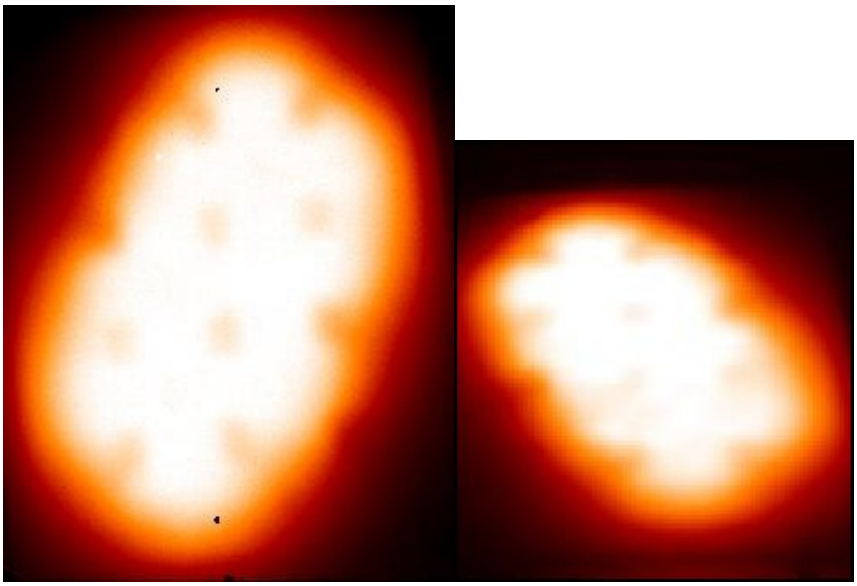

Fig. 2.6: 30 and 50% full respectively.

at these locations. This demonstrated that some vapor was evaporating near the evaporator and moving away from the evaporator to condense everywhere else. These are important observations because our MathCAD model does not take into account the volume of fluid needed to sufficiently supply the panel to maintain the circulation.

The results of the 20% tests were better. Almost the entire panel was within $5°C$ temperature difference, and there were no dry areas or posts. Fluid was observed to flow around the supports and drip from the top surface to the bottom. The temperature was lower across the panel than in the 30 and 50% tests. As we increased the volume of fluid to 30 and then 50%, less and less of the panel was isothermal. In the 30% test the higher temperatures and larger gradients are likely due to the additional thermal resistance of the liquid rather than a change in curvature. Slightly higher maximum temperatures were recorded across the panel during both the 30% and 50% tests than in the 20% test. The bubbles were visible over the evaporator during the 50% test.

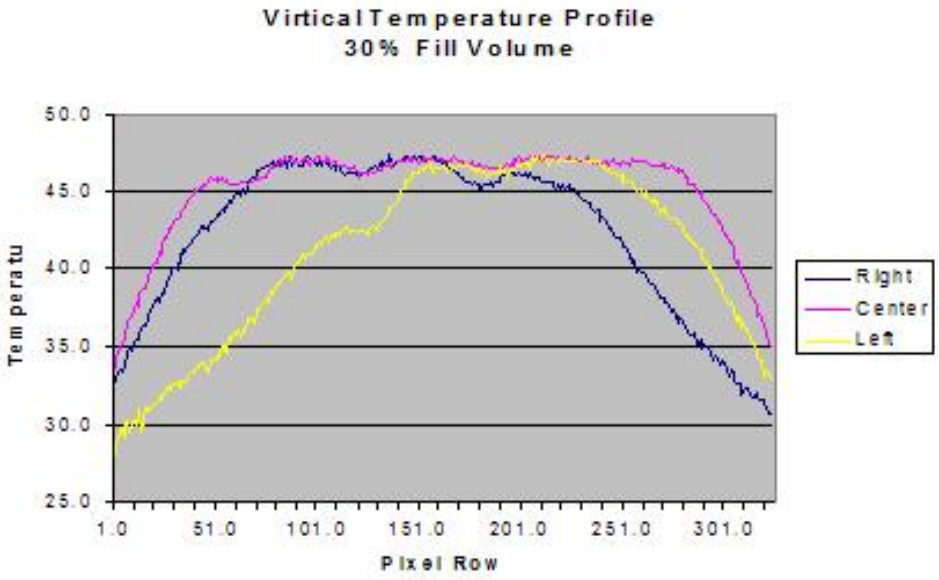

Fig. 2.7: 30% fill temperature profile.

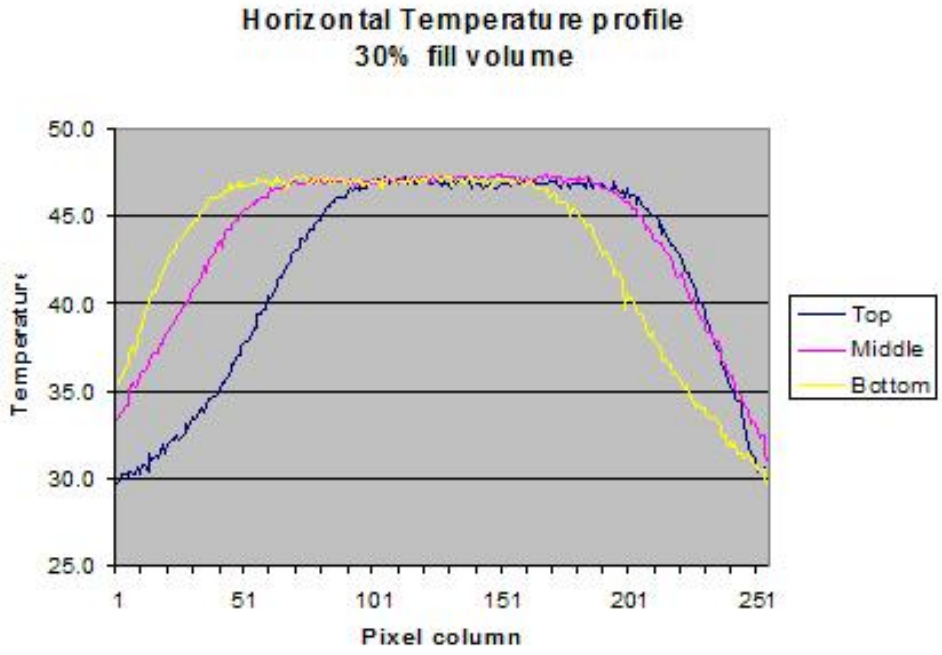

Fig. 2.8: 30% fill temperature profile.

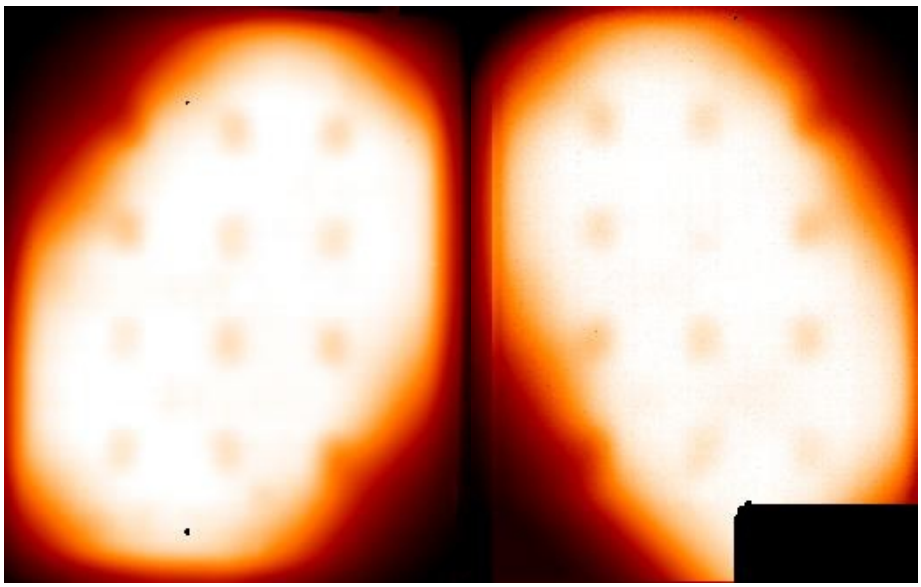

Fig. 2.9: Two 20% tests.

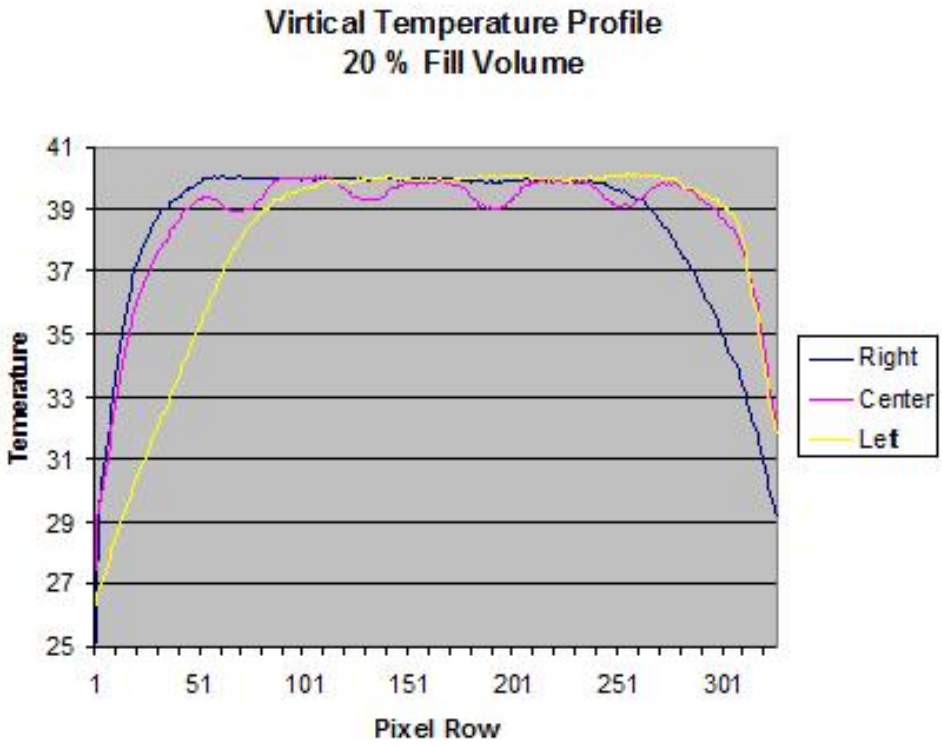

Fig. 2.10: 20% fill temperature profile.

2.1.2 Conclusion on Effect of Fluid Level

The formation of bubbles indicates the onset of nucleate boiling which can aid the heat transfer process unless the bubbles grow too large before bursting or if there are too many bubbles forming over the surface of the evaporator. The curvature in the 50% and 30% fill tests was smaller because the grooves were almost completely full. It may be that the smaller curvature decreased the capillary pressure resulting in less mass flow rate off that surface and the associated rise in temperature at that location caused ΔT_{excess} to be larger than in the 20% charge test. This change in ΔT_{excess} could indicate a decrease in the convective heat transfer coefficient. However, it is also possible that the increase in ΔT_{excess} is due only to the increase in thermal

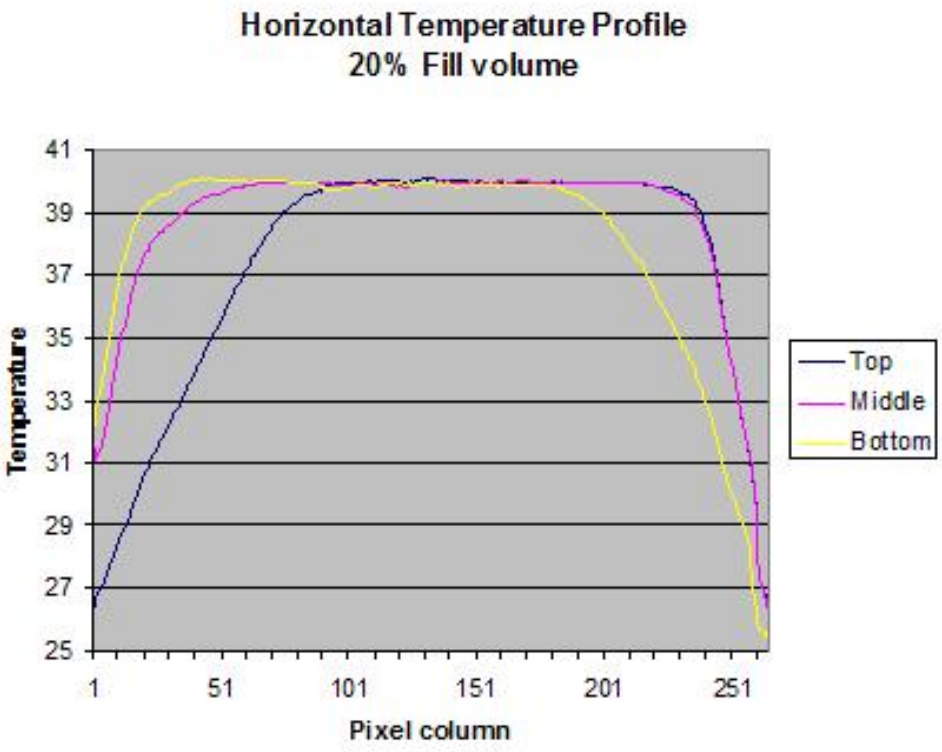

Fig. 2.11: Horizontal 20% fill temperature profile.

resistance of the liquid. From the results of these tests it seems that the charge volume does affect the maximum temperature, and the thermal gradient across the panel. However, it remains unclear whether this is due to the depth of the liquid, or the curvature of the meniscus or both. In either case it is apparent that the volume of liquid used in channel panels affects the heat transfer coefficient of the evaporator.

2.2 A Modified Hubbard Model

In the year 2001 Neal Hubbard proposed a model [6] to predict the behavior of channel panel FPHP's as part of the beginning stages of the current and ongoing project to develop the technology. At that time the goal was to make a channel panel from carbon composite material which was to axially conduct the heat. The geometry

of this channel panel did not include the two-dimensional pattern of grooves but only axial grooves and was approximately 1cm x 10cm x 100cm with heaters located on the top and bottom at one end and the condenser located on the top and bottom at the other end. The Hubbard model was based entirely upon the work of G. P. Peterson [2], who has published several works on the design and modeling of heat pipes, and appropriate changes were made to the equations presented by Peterson to accommodate the geometry of the panel. The model estimates the operating limits of the panel as a function of saturation temeprature. Recall from 1.1 that the five limits are the capillary, boiling, sonic, entrainment, and viscous limits. In that section we discussed that only the sonic, capillary, and boiling limits are needed for the design of a channel panel. The entrainment, and viscous limits will be calculated as part of the design output but the equations are not discussed in this paper. The equations for the sonic, capillary, and boiling limits can be found in 1.1. Testing of the carbon composite panel revealed that the model reasonably predicted the temperature drop and provided enough controls that a panel could be designed so that the operation limits would meet design requirements. However, testing of the panel did not verify that the model accurately predicted any of the operating limits and the overall heat transfer coefficient was not acceptably accurate. More investigation is required to show that this model can accurately predict the operation limits.

2.2.1 Changes to the Hubbard Model

The equations defining overall heat transfer coefficient and equivalent conductivity are well established. The inaccuracy of the prediction by the Hubbard model lies only in what values have been used in those equations. Equations 2.5 and 2.6 are the equivalent conductivity of the panel derived from Fourier's Law of conduction and

the overall heat transfer coefficient from Newton's Law of cooling as represented in the Hubbard Model.

$$h_{pc} = \frac{1}{A_p \cdot R_T} \tag{2.5}$$

$$k_{eff} = \frac{L_{eff} + t_p}{A_p \cdot R_T} \tag{2.6}$$

where R_T is the thermal resistance, A_p is the cross-sectional area of the panel, and $L_{eff} + t_p$ is the distance across and through the panel which the heat must travel respectively. In the case of a heat spreader which changes how the effective length is calculated a FPHP may locate the condenser directly across the thickness of the panel from the heater and cover a larger area than the heater. This means that the equation to calculate the effective length given in the Hubbard model is not always correct because the adiabatic section is the thickness of the vapor space rather than part of the radial distance from the heater to the wet-point of the condenser. As we can see in the equation for the overall heat transfer coefficient h_{pc} the cross-sectional area A_p of the panel is used which is only weakly justifiable for a heat pipe because the A_p is not the heated area of the evaporator inside the panel. Newton's Law of cooling defines the area term as the heated (or cooled) area where the fluid undergoes some change in heat energy and not simply the area through which the fluid passes. Finally, the application of these equations to values as elusive to define as "equivalent conductivity" and "equivalent heat transfer coefficient" leave them as little more than qualitative evaluations of a model. Improvements will be limited to changing the parameters used to be more defensible but Equations 2.5 and 2.6 will not be used to describe any real properties observed in experimentation.

The revised Hubbard model will be referred to as the Hubbard-Harris model. The Hubbard-Harris model is essentially the same as the original Hubbard model

except where geometry parameters are defined, calculated, and used. In the Hubbard model the term A_e refers to the evaporator area, but this could be several values depending on the environment. In order to eliminate the ambiguity two new terms A_{heater} and A_{wev} now define the surface area of the heater on the outside of the panel and the surface area inside the panel under the heater footprint respectively. Notes have been added to emphasize the need to make changes where appropriate such as in the capillary pressure equation where gravity may assist the liquid flow back to the evaporator and so should enhance the FPHP capabilities rather than hinder. Other changes reflect similar need for flexibility, and also to use the appropriate values in each equation. A copy of the MathCAD program will be included in a CD that will accompany this document.

2.2.2 Testing

Two channel panels were designed using the Hubbard-Harris model and tested to show that the model would accurately predict the heat transfer coefficients, overall temperature drop and either the capillary limit or boiling limit. The first prototype was made from polycarbonate (Lexan). Remember from Equation 1.9 that the boiling limit is reduced by materials with a high thermal resistance. Polycarbonate was chosen for its transparency, and its high thermal resistance so that the boiling limit could be reached at a reasonably low heat input. The dimensions of this channel panel are 20 cm x 25.3 cm x 1.4 cm where the thickness of the walls was $0.4cm$ through the thickness of the panel. The panel heaters were placed in the center of the panel across the width of the vapor space on the bottom of the panel. The panel was exposed to ambient air at $20°C$ on all sides except the bottom where a large foam insulator prevented the heat from escaping except by moving through the panel first.

Due to the high thermal resistance of polycarbonate the local effect of the heater on a thermocouple measurement taken adjacent to the heater will be negligible so that this measurement can be assumed to be the temperature of the panel at that location. Similarly, for the measurements taken on the exposed surface where each thermocouple was covered by a piece of aluminum tape with acrylic adhesive these measurements can be assumed to be the temperature of the external surface of the panel at these locations. A summary of the panel geometry is shown below with the prediction of the lowest operating limit, which is the boiling limit. A_p is the cross-sectional area of the width of the panel $w_p \cdot t_p$.

$$\begin{array}{cc} \delta = 2mm & t_v = 2mm \\ \omega = 1mm & L_{eff} = 0.085m \\ w_v = 173mm & w_p = 0.181m \\ A_{condenser} = 0.04m^2 & t_p = 0.014m \\ A_{heater} = 0.002m^2 & A_p = 2.534e^{-3}m^2 \end{array}$$

$T_{sat}(K)$	$Q_b(W)$
300	118.1
310	70.7
320	44.1
330	28.3
340	18.7

The second prototype was designed for copper with smaller channels and a larger length to width ratio. This was done so that the capillary limit could be more easily

tested and compared to the model prediction. The panel is 7.62 cm x 30.6 cm x 0.5 cm with a wall thickness of $0.1cm$.

A summary of the panel geometry is shown below with the prediction of the lowest operating limit, which is the capillary limit. The heat flux will be used here and is the power at the limit divided by the area of the heater.

$$\delta = 1mm \qquad t_v = 0.75mm$$
$$\omega = 0.8mm \qquad L_{eff} = 0.241m$$
$$w_v = 55mm \qquad w_p = 0.076m$$
$$A_{condenser} = 5.588e^{-3}m^2 \qquad t_p = 4.75e^{-3}m$$
$$A_{heater} = 1.93e^{-3}m^2 \qquad A_p = 3.619e^{-4}m^2$$

$T_{sat}(K)$	$Q_c\left(\frac{W}{cm^2}\right)$
320	1.19
330	1.68
340	2.33
350	3.09
360	4.00

2.2.2.1 Polycarbonate Panel

The test was carried out by incrementally increasing the power to the heaters to approximately half the expected limit where the panel was allowed to reach steady state. The panel was observed to be working properly with no bubbles present. Measurements were taken to know the approximate area of the exterior condenser surface where the heat was convected away from the panel. This was decided to

include all area within $10K$ of the temperature of the surface directly opposite the heaters. Then the power was increased by increments of 1 or 2 watts until the evaporator was observed to dry out. In the middle of the test the thermocouple on the heaters was accidentally jostled out of place so that its sensor was in contact with the heaters. The thermocouple was carefully moved back to its proper position without moving the panel. Following this the power was increased as before and at approximately $17.0W$ the bubbles were noticeably larger and more rapid. It is difficult to accurately determine the exact onset of nucleate boiling in ethanol because the bubbles formed are very small. However, it is reasonable to assume, given these observations that the boiling regime at $17.0W$ was well within the nucleate boiling and probably nearing the jets and columns region. At $20W$ part of the evaporator was visibly dry at the center of the associated heater and at $21W$ two of the four heaters were showing signs drying out. The test was continued to $23W$ where all four heaters were at least partly dry and the first heater was entirely dry. Since each heater occupied a different position on the panel we can see that different heaters would experience dry-out at different rates due to small differences in the grooves feeding liquid to the heaters. Figure 2.12 is a plot of the temperature vs. time and notes have been added for clarity.

The model also predicts that the panel will reach the boiling limit near $20W$ for a saturation temperature near $340K$ or $67°C$. Our thermocouple data shows that the top surface of the panel, which is the condenser, opposite the heaters was at $48°C$ and the temperature adjacent to the heaters was $138°C$ when the panel was powered at $20W$. Since the polycarbonate is a resistant material the interior temperature of the vapor space T_{sat} must be verified by calculation. The boiling limit, as defined by Equation 1.9, correlates the liquid properties, the wall/surface properties, and the capillary pressure at the nucleation site. Equation 1.9 predicts the power necessary to

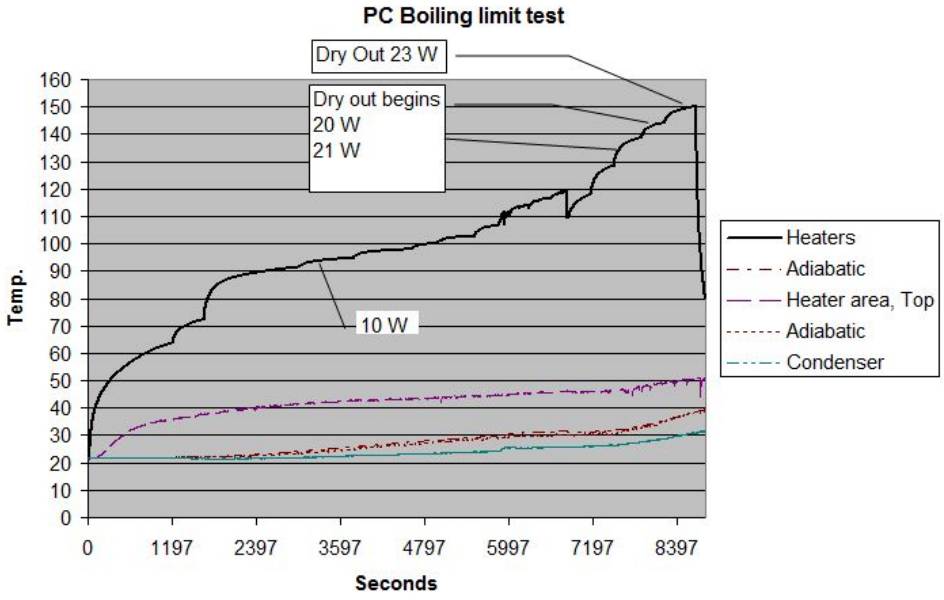

Fig. 2.12: Polycarbonate panel boiling limit test.

evaporate more liquid at the nucleation sites than can be supplied to the nucleation sites. In shallow pool boiling the observation of the CHF condition is different than in normal pool boiling where a vapor bubble covers the surface of the heat source. Gu made the following observation of the CHF for FC-72, "5) No stable vapor domes were noticed for the liquid FC-72 in the level range from $10mm$ to $0.5mm$," [17, pg. 117]. For shallow pool boiling the CHF condition may be observed by the sudden increase in temperature for a small increase in power, or recording the temperature and power where the evaporator becomes dry. This means that in shallow pool boiling the usual visual evadence of the CHF condition may appear to be the same as when other limits are reached, such as the capillary limit. Therefore, "dry-out" of the evaporator can be observed visually and used to visually identify when the CHF has been reached.

I will show that the T_{sat} is between $330 - 340K$ by calculating the temperature drop through the panel wall from the heaters to the vapor space and also from the condenser surface to the vapor space using the 1-D conduction equation. The fol-

lowing assumptions have been made for the physical condition of the panel at $20W$ based on observations.

- The saturation temperature is the same everywhere in the vapor space of the panel; a 1-D analysis is therefore appropriate and Fourier's Law of conduction will be used.
- Part of the surface of the evaporator is dry and so the vapor touching the surface of the evaporator is very close to the temperature of the surface. I can therefore consider the bulk resistance of the wall material, find the temperature drop ΔT and from the data take the surface temperature adjacent to the heaters to find T_{sat}.
- The vapor was very close to the surface of the condenser because gravity drained any liquid away from the top surface quickly. Therefore we can also assume that the T_{sat} is very close to the temperature of the condenser surface.
- The area term in the conduction equation is for each case the surface area of the surface where the heat is removed from the control volume. That is the inside surface of the evaporator which includes the surface area of the grooves and the outside surface of the condenser which does not have grooves. The control volume is separate for each case.

The values of the terms for the 1-D conduction equation are summarized below with the experimental data and predicted T_{sat}. In addition to the surface area of the grooves in the evaporator it was recognized that the heat would spread out slightly as it passed through the wall material and more surface area on the inside of the evaporator would participate in the heat transfer. An angle of 45° was assumed so

that the width of the "border" area around the heated wick would be the same as the thickness of the wall material. The total surface area of the grooves in this border is not included because the thermal resistance of the polycarbonate makes it difficult to know exactly how far the heat will penetrate laterally. L_e and W_e are the length and width of the evaporator respectively, k_{pc} is the conductivity of polycarbonate, and T_e is the temperature of the panel immediately adjacent to the heaters on the outside of the panel. A_{ge} is the surface area of the posts in the evaporator without the tops of the posts and is not the same as A_{wev}, it is $A_{wev} + A_{border}$, Figure 2.13.

$$A_{ge} = 5.3e^{-3}m^2$$
$$L = 0.004m$$
$$k_{pc} = 0.194\frac{W}{mK}$$

$$Data$$
$$T_e = 138°C$$
$$\Delta T = 78°C$$

$$Predicted$$
$$T_{sat} = 60°C$$

The values of the terms for the 1-D conduction equation are summarized below with the experimental data and predicted T_{sat}. The surface area where the heat leaves the control volume is the outside surface of the panel where there are no grooves. The surface area is calculated from the width of the panel multiplied by the length of the panel which was within $10K$ of the temperature of the condenser surface directly

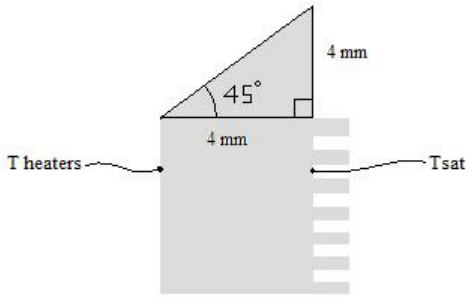

Fig. 2.13: Heated area diagram.

opposite the heaters. The length was measured during the test at a steady state power of 10 W, see Figure 2.2.2.1. The term A_{sc} is the outside surface area of the condenser.

$$A_{sc} = 2.58e^{-2}m^2$$

$$k_{pc} = 0.194\frac{W}{mK}$$

$$L = 0.004m$$

Data

$$T_c = 48°C$$

$$\Delta T = 16°C$$

Predicted

$$T_{sat} = 64°C$$

As we can readily see the two calculations agree reasonably well with each other and both lie between 330 and 340 K. If we interpolate the predicted power limit from

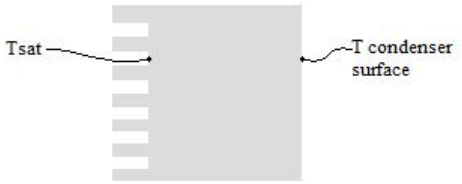

Fig. 2.14: Cooled area diagram.

the model with these temperatures we will find that at $64°C$ the power limit should be near $21.6W$ that is in good agreement with the original heat of $20W$ used in the calculation and the experimental results where the boiling limit was reached between 20 and 23 watts.

2.2.2.2 Copper Panel

The copper panel was powered in a similar manner as the polycarbonate panel though as is shown in the operating limit prediction the units are in $\frac{W}{cm^2}$. The temperature drop through the panel wall should be roughly the same for any point that is outside the heated or cooled area. Given the thinness of the copper panel wall this temperature drop should be very small. This means that the saturation temperature of the vapor inside the panel should be very near the surface temperature of the panel in the adiabatic zone. This assumption was not valid for the polycarbonate panel because of the very low conductivity of the material. Some deviation of the model from the experimental results is expected because the copper panel was fabricated with V-shaped channels rather than rectangular. Currently the model does not have an option for other channel cross-sections.

The copper panel was powered $4 - 50W$ by a 1" X 3" Minco Thermofoil heater. The panel was allowed to reach steady state for each new heat flux applied. The adia-

batic temperatures, the temperatures around the heater, and the heater temperature were averaged and this value used as an estimate of the film temperature of the evaporator surface. The difference $T_{sat} - T_f$ is assumed to be near the actual ΔT_{excess}. Other locations are also differenced with T_f to show whether those locations have partly or completely passed an operation limit. As with the polycarbonate panel we can expect to see individual points reach the operation limit at different times.

As we can see in Figure 2.15 the change in temperature of the corner area rises approximately $0.5\frac{K}{W}$ or less until the power is set to $50W$ where the rise in ΔT_{excess} is $5K$ for $6W$ or $0.83\frac{K}{W}$ that indicates the limit is reached. The heat flux at $50W$ for this heater is $2.55\frac{W}{cm^2}$ and the $T_{sat} = 66°C = 339K$. The model predicts a heat flux of $2.33\frac{W}{cm^2}$ at $T_{sat} = 67°C = 340K$. Figure 2.16 shows a comparison of the data with the prediction of the Hubbard model for capillary limit, where the limit was reached at approximately $1.5\frac{W}{cm^2}$. The apparent discrepancy can be explained by noticing in 2.15 there are two changes in the slope of the temperature curve. The first occurs near the predicted operation limit of $1.5\frac{W}{cm^2}$ and the second when the corners are completely dry. This indicates that there can be a significant change in power density as the evaporator continues to dry-out.

I also observed that for low power input the channel panel will not display the characteristic isothermal zone when the cooler is set to a constant temperature for all heat inputs. This is due largely to the much higher rate that heat can be removed by the cooler as compared to the rate which heat is added to the panel. Thus it is possible for the wet point to be coincident with the heater. Also, non-condensible gases can block the condenser increasing the temperature gradient in the FPHP. Figure 2.17 shows three temperature profiles from the corner sensors by the heater to the edge of the cooler platen.

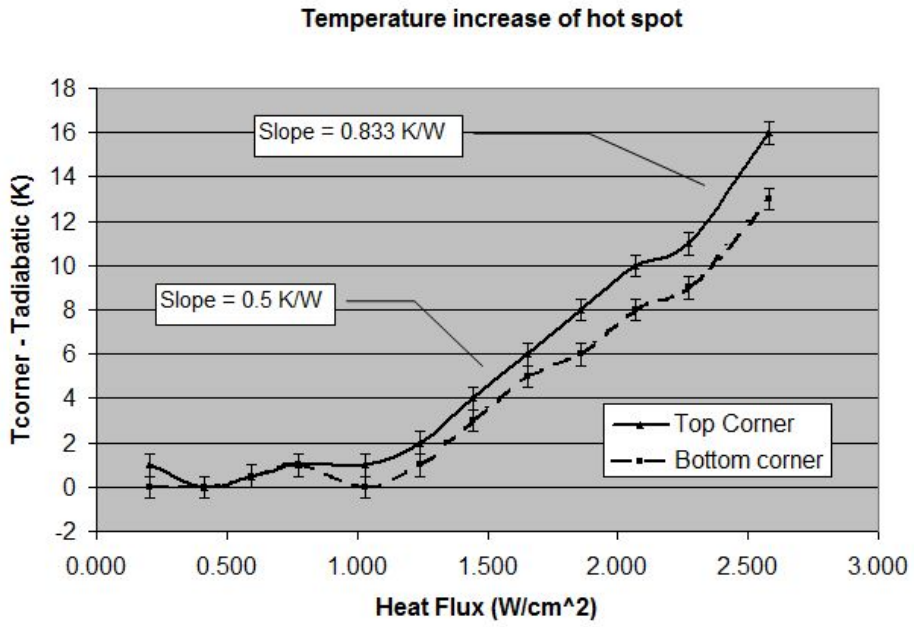

Fig. 2.15: Difference of corner and adiabatic temperatures vs. heat flux.

2.2.3 Conclusion on the Hubbard-Harris Model

The Hubbard-Harris model has been shown to accurately predict the boiling limit for heat transfer through a channel panel heat pipe at the correct saturation temperature. For any channel panel with a constant cooler temperature there is a lower limit to the usefulness of the channel panel as a heat transfer device. As a conceptual tool the Hubbard-Harris model will be useful in preparing for the preliminary design phase of a channel panel flat plate heat pipe and any necessary prototypes. Furthermore, this model can be used as a teaching tool to familiarize the engineer with FPHP parameters.

2.3 Experimental Verification of h_{boil} Using the Copper Channel Panel

To test the conclusions from Figure 1.2, the copper panel was tested several times

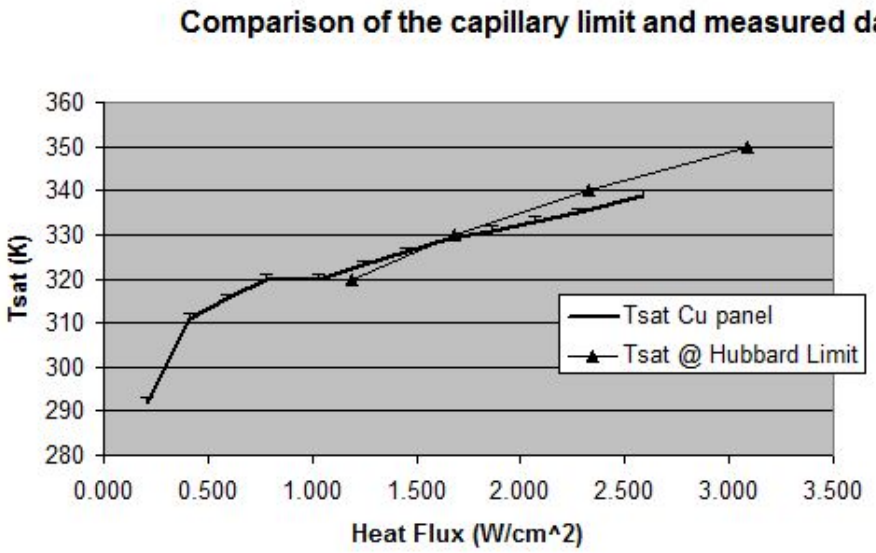

Fig. 2.16: T_{sat} Copper panel compared to Hubbard Model capillary limit prediction.

with changes to various parameters the most important of which are the heat flux and charge volume. The panel was tested in what I term the conductive mode and also in the convective mode (or alternatively the spreading mode). That is the conductive mode places the heat source and cooler at extremes from each other so that the evaporated fluid must flow axially through the cross-section from the heat source to the cooler and the panel is insulated everywhere for the test. The convective mode places the heat source across the thickness of the vapor space from the cooler and is insulated everywhere else. The purpose of these two different tests is to show that the average convective coefficient h_{boil} calculated from Equations 1.14 and 1.13from 1.2 can be used for both the conductive and convective mode.

2.3.1 Conductive Mode Test

Tests were performed on the copper panel in the conductive mode for various power levels at a constant cooler temperature, and charge volume. The saturation

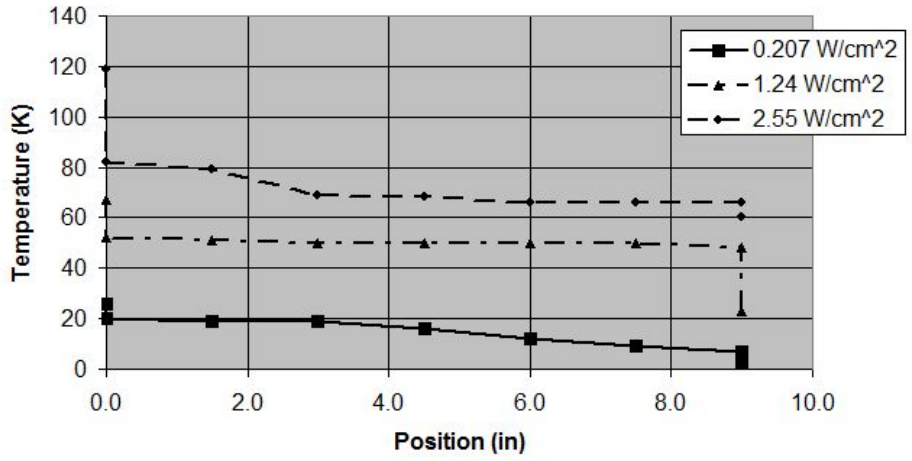

Fig. 2.17: Temperature profile vs distance form evaporator center for different heat fluxes.

temperature, and the temperature of the surface of the evaporator can be estimated from the data. Large temperature gradients can exist between the heater and the panel surface, and also between the cooler and the panel surface due to joint resistance. In order to mitigate the effect of temperature gradients imediately surrounding the heater in my analysis, the temperatures around the heater, and in the adiabatic section were averaged to estimate the surface temperature of the evaporator inside the panel. This method weights the adiabatic section surface temperature, which is close to the saturation temperature, more than the other temperatures because the saturation temperature at these heat fluxes should be close to the surface temperature at the evaporator surface. The temperature drop through the panel wall should be roughly the same for any point which is outside the heated or cooled area, and given the thinness of the copper-panel wall this temperature drop should be very small. This means that the saturation temperature of the vapor inside the panel should be very near the surface temperature of the panel in the adiabatic zone. These values result in a power-ΔT_{excess} relationship from which a convective heat transfer coefficient

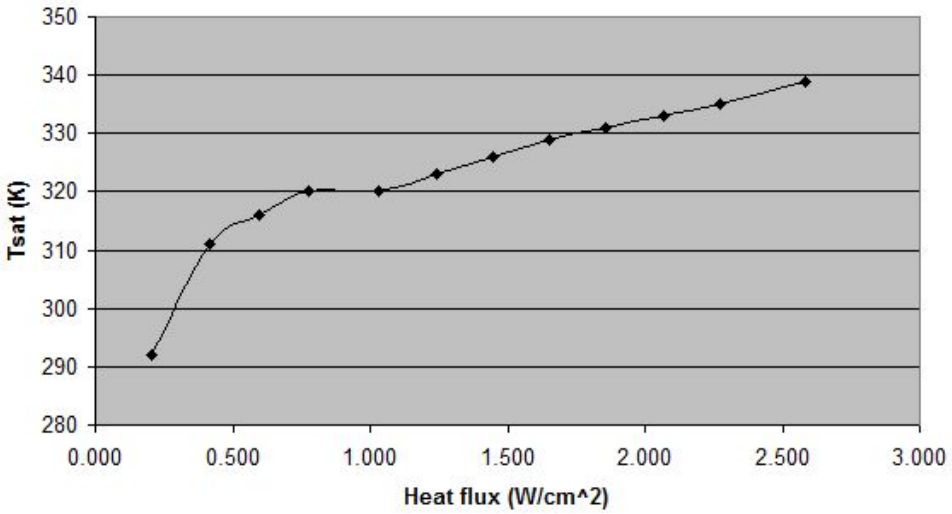

Fig. 2.18: Saturation temperature vs. power.

h_{boil} can be estimated. Also, the wet point of the condenser is assumed to be where the temperature of the panel surface suddenly changes to a lower value than the adiabatic temperature by more than $2°C$ from one PRT to the next. This is because the adiabatic section should not change temperature greatly in a functioning and insulated channel panel. Since the placement of the PRT's may not be directly over the wet point each time the wet point temperature will be calculated as the average between the adiabatic and the next lowest temperature reading. Once the adiabatic temperature is identified the boundaries of the zone should be easily identifiable and also the approximate location of the wet point of the condenser.

The charge volume in these tests was 30% of the total volume inside the panel which results in a liquid height of approximately $0.5mm$. The shallow pool boiling Equations 1.13 and 1.14 predict the critical heat flux from which an average h_{boil} can be obtained.

Using the values in Table 2.1 and the heat flux of each test I calculated an estimated ΔT_{excess} for each power setting and compared that value to the actual

Table 2.1: Predicted Critical Heat Flux and Convective Heat Transfer Coefficient

$T_{sat}\,(K)$	$Q_{crit}\left(\frac{W\cdot 10^3}{m^2}\right)$	$h_{boil_{av.}}\left(\frac{W}{m^2K}\right)$
320	13.07	4355
330	15.75	5254
340	18.74	6245
350	21.88	7292

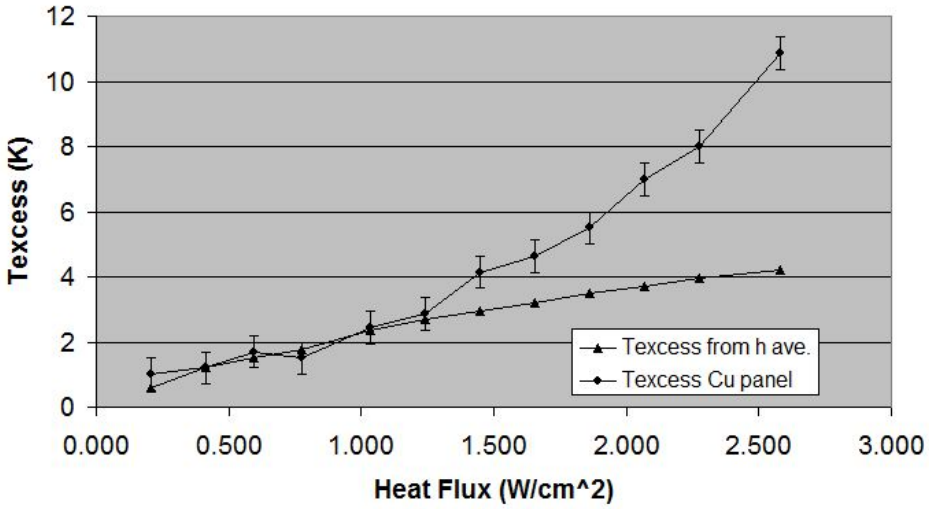

Fig. 2.19: Comparison of predicted and measured ΔT_{excess} vs. heat flux.

recorded temperature drop from the test data. Notice the approximation error grows as the panel passes through the capillary limit where the heat transfer coefficient can no longer be approximated by and h_{boil}. The temperature of the heater surface, which is still wetted, can be estimated as before by the average of the temperatures around the heater, the heater, and the adiabatic temperature measurements.

2.3.2 Conclusion

The figure shows reasonable agreement between the experimental and analytical results based on Gu's model. The $h_{boil_{av.}}$ obtained from the shallow boiling CHF Equations 1.13 and 1.14 are a good approximation of the boiling heat transfer co-

efficient of the liquid in the evaporator below the operating limit. The results of Chuanbao Gu's work indicate that the channel panel surface geometry increases the CHF and also reduces the point where nucleate boiling begins. The nucleate boiling regime is therefore larger and the heat transfer coefficient will be more constant which further improves the accuracy of $h_{boil_{av.}}$ for the nucleate boiling curve up to the CHF. As discussed in section 2.2 for a constant cooler temperature FPHP's may not be sufficiently powered to display the characteristic isothermal zone due to the disparity between the heat input and the cooling capacity of the cooler. This is important to remember for design because an underpowered FPHP will not provide a thermal advantage to the user. In this situation h_{boil} may not be accurate though no trials were attempted because of the lack of utility of the operating condition.

2.4 Joint Resistance

Channel panels must be integrated into larger thermal management systems through joints or points of contact between the Channel panel and the rest of the system. Other investigations have shown that the largest temperature drop in a heat pipe usually occurs in the evaporator between the source and the interior surface of the heat pipe. Part of the design process will be to determine what, if anything, needs to be done to minimize the temperature drop between the hot device and the panel wall.

2.4.1 Spreading and Joint Resistance Model by M. Bahrami

There is a complicated network of thermal resistances wherever heat moves across a joint from the source to the Channel Panel or from the Channel Panel to the cooler.

This is called joint resistance. The joint resistance is comprised of two parts. The first is the bulk resistance of the material, easily recognized from Fourier's law of conduction [20].

$$R_b = \frac{t}{A_a k_p} \tag{2.7}$$

where t is the thickness of the medium and A_a is the area through which the heat moves and k_p is the conductivity. The second is the spreading resistance and is the temperature drop over the joint interface divided by the power input.

$$R_s = \frac{\Delta T}{Q} \tag{2.8}$$

$$R_j = R_s + R_b \tag{2.9}$$

A paper by Fuller and Marotta [21] provides equations to predict the joint resistance of rough surface polymer-metal joints. Fuller uses the following premise about the operating condition of the plastic.

> (1) 1D heat transfer and that the heat flow passes through the contact plane with the heat flow direction perpendicular to the contact plane; and (2) the equivalent contact simplification. The contact plane or the apparent area is the projection of contacting surfaces on the plane normal to the direction of the applied load, thus the real contact area is always less than, or at its limit, equal to the apparent area.[20, pg. 24]

While Fuller and several sources suggest that these premise are not correct the correlation for the bulk resistance to experimental data is sufficient to justify its use in thermal system design. Bahrami developed an equation to predict the spreading

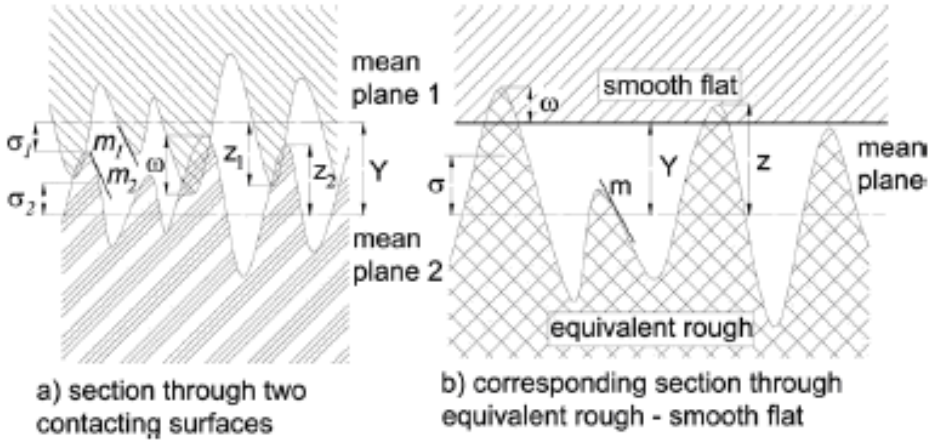

Fig. 2.20: Equivalent contact of conforming rough joints [20].

t_o	Thickness of substrate
P	Joint Pressure
E_p	Modulus of elasticity of the joined part
H_{mic}	Microhardness of the joined part
σ	Surface roughness of the joined part
m	Correction factor
k_s	Thermal conductivity of the substrate
F	Joint Force

Fig. 2.21: Nomenclature.

resistance R_s that also works very well. The conditions for the use of these two equations together are (1) the mean joint temperature is less than the polymer glass temperature and (2) the deformation mode of the asperities is plastic.

$$R_b = \frac{t_o\left(1 - \frac{P}{E_p}\right)}{A_a k_p} \tag{2.10}$$

$$R_s = \frac{0.565 H_{mic}\left(\frac{\sigma}{m}\right)}{k_s F} \tag{2.11}$$

$$R_j = \frac{0.565 H_{mic}\left(\frac{\sigma}{m}\right)}{k_s F} + \frac{t_o\left(1 - \frac{P}{E_p}\right)}{A_a k_p} \tag{2.12}$$

2.4.2 Conclusion for Joint Resistance Model

Bahrami uses this model to accurately predict the joint resistance of a polymer-metal thermal joint in a vacuum. In channel panels generally metal-metal contact will be made between the heat source and the panel. Bahrami says in his summary, "The present model assumes that the mechanical behaviors of polymers are similar to metals for temperatures below the glassy temperature" [20, pp.26]. Since the equations function only in this mode for polymers and metals have no glassy temperature, they will work similarly for metals and can be used for this critical joint in channel panel design.

Chapter 3

Fabrication and Assembly

Fabrication of any FPHP is challenging. The geometry is usually very simple, however, in order for the FPHP to function the design and manufacturing must provide a means to meet the requirements explained in Figures 3.3 and Section 3.4. This means providing a way to access the interior space of a FPHP without compromising the ability to hermetically seal the FPHP from the outside. Other issues with materials increase the difficulty in machining parts and joining panel parts hermetically, for example, aluminum is difficult to weld. Largely the results of this part of the study are qualitative because the evaluation of the methods used to join the parts and access the interior space for filling is Pass/Fail. That is either the panel passed a leak check or not and the filling port was sealable or not. The panels used in this part of the study are not full channel panel prototypes but rather blanks only.

3.1 Material Selection

Material selection is one of the more important decisions in Channel Panel design. However, the myriad of possibilities leave little more than general guidelines for what is "best" but the demands on the channel panel by the customer will leave few viable material candidates so once the short list has been created by the customer, selection of the best material should become fairly simple.

Table 3.1: Material Compatibility with Some Common Liquids

Fluid	Materials Compatible	Materials NOT Compatible	Flammibility	Hazards	Notes
Ammonia	Aluminum, ferritic steel, stainless steel, most	Brass, copper, most elastomers	DOT: Non-flammable gas	Innhalation and bodily contact	High pressure (10 atm) at 300 K;
Butane	Aluminum, brass, copper, ferritic steel, stainless steel, plastics	Some elastomers	DOT: Flammable gas	Fire	Risk of corrosion by impurities in presence of water
Carbon Dioxide	Aluminum, brass, copper, stainless steel,plastics	Ferritic steels, elastomers	DOT: Non-flammable gas	High pressure and inhallation	Causes cold brittleness and can corrode ferritic
Ethane	Aluminum, brass, copper, ferritic steel, stainless steel, plastics	Some elastomers	DOT: Flammable gas	Fire	
Methane	Aluminum, brass, copper, ferritic steel, stainless steel, plastics	Most elastomers	DOT: Flammable gas	Fire and high pressure	Risk of corrosion by impurities in presence of water
Methanol	Ferritic steel, stainless steel	Aluminum, brass	DOT: Flammable liquid	Fire and poison	
Oxygen	Aluminum, brass, copper, ferritic steel, stainless steel	Ferritic steels, plastics, elastomers	DOT: Non-flammable gas	Fire and high pressure	Corrosive in presence of water
Propene	Aluminum, brass, copper, ferritic steel, stainless steel, plastics	Elastomers	DOT: Flammable gas	Fire	Risk of corrosion by impurities in presence of water
Water	Platics, Brass, Copper	Slight corrosion with Aluminum			

- Choose a list of materials which are common to the industry where the Channel Panel will be applied.

- The material must be compatible with the working fluid so that there will not be any corrosion of the panel structure. Fortunately, the compatibility of liquids with the most utilized materials in thermal management is well known and documented. Table 3.1 summarizes the compatibility of several materials and common liquids.

Efficiently placing a two-dimensional grid of channels onto a sheet of material presents a multitude of challenges and I will not attempt to describe all the possible difficulties or advantages of materials and methods which can produce such a geometry. The quality of the grid making process should be sufficient only to promote good fluid flow, heat transfer, and cleanliness of the panel.

- The machinability of the various materials must be considered when attempting to cut the channels into a part.
- If the channels are to be fabricated by depositing posts onto the surface rather than cutting part of the surface away then the strength of the bond between the deposited post and the surface must be enough to prevent debonding if the panel is shocked, shaken or if the panel walls are deformed by internal pressure.
- The required lifespan of the panel may require that some materials be used over others because of degradation in the material, or of the joints holding the different parts of the channel panel together.
- The material must not deform greatly, melt, burn, or out-gas when operating at the maximum temperature of the heat source.
- The lead time on channel panels can be large if the materials and/or the importance of the channel panel is high. Each channel panel is designed to work within a specific envelope of temperatures.
- If the best material for the application is too costly either for the bulk material or in machining time and complexity then less advantageous materials must be used.

Materials of choice in thermal management are copper and aluminum for their high conductivity. Some other important metals are Titanium, Beryllium and other metals common to the electronics industry though they are not common for FPHP's. These materials should always be the first candidates for any channel panel application because they have well understood properties, and are reasonably common. Composites or plastics may become more important as they are developed to have

higher thermal conductivity, in the $30 - 40\frac{W}{m \cdot K}$ range, while maintaining their electrical resistivity, and light weight, a valuable property for a FPHP.

3.2 Joining

After the various panel parts have been fabricated these parts have to be assembled in a way which permanently seals the interior space of the panel. The methods evaluated to assemble the panel were gluing, soldering, brazing and welding. Aluminum, copper and some plastics were used as the materials for these studies. Other materials could be more advantageous for some of these processes however the materials mentioned above are the more important to the thermal management industry. Aluminum is especially important for its low mass and high conductivity.

3.2.1 Joining with Adhesive Processes

In general the gluing of any material follows the same steps as with other materials. The surfaces must be prepared by any of several methods that clean the surface of contaminants and create a uniform roughness. This can be done by sanding, sandblasting, grinding, and chemical etching depending on the material though, sanding and chemical etching produce the best results with the lowest impact on the integrity of the part. Following this step an adhesive is mixed with its hardening agent. In order to maintain the bond line thickness some kind of small grit, usually .005" glass spheres, is mixed with the adhesive. Then the adhesive is applied evenly and the parts clamped together firmly until cured. Then a post cure is usually performed to ensure the strength of the bond. Two glues were evaluated and the properties of each were taken into account. The first was Epybond 1210A and the second Hysol EA 9309.2na. Surfaces were sanded and others were etched resulting in some improve-

ment of an etched surface over the sanded surface. Either adhesive works reasonably well but Hysol can work to a higher temperature. One final advantage is that a glued panel, if the seal be broken, can be cleaned, and repaired with the same parts.

Gluing as a method of assembly for channel panels is problematic but useful. With plastic panels gluing is fast and fairly reliable. Since plastics typically have thermal conductivities $0.1 - 1.0 \frac{W}{m \cdot K}$ the boiling limit will be so low that the panel is not likely to develop enough internal pressure to burst the seal. More likely is that the outside wall of the plastic panel will melt before the saturation pressure inside the panel becomes very much higher than 1 atm. This depends on the working fluid but usually water, isopropanol, or ethanol are used which have high enough boiling points to make this a reasonable guideline for plastic panels. There are some plastics which have been recently developed that are electrically insulative but thermally conductive. To avoid bursting the panel these as well as carbon composite materials will require more bond area. Gluing has been somewhat successful for metal panels as long as the saturation temperature did not rise above the boiling point of the working fluid at 1 atm. Gluing is problematic because the bond of the adhesive can degenerate over time resulting in a rupture in the seal, and/or alcohols may attack the adhesive if alcohols are used as working fluids or cleaning agents. This happens even when precautions have been taken to ensure that the working fluid remains below 1 atm. Adhesives have a tendency to run into and block some of the channels near the joints of the panel and usually have low conductivities each of which reduces the effectiveness of a panel.

3.2.2 Soldering

Soldering proved to be a very reliable method for assembling metal panels. A

copper panel was easily soldered and sealed using tin lead 1/16" solder and Kester flux # 186 for the copper-copper joints and copper-steel joints used Indaloy Flux # 3 with tin zinc solder. The heat source was a propane torch and heating of the panel wall material was kept to a minimum due to the relatively low melting point of the solder. The soldered joint of this panel was later intentionally broken in a test and afterwords was repaired with equal success by the same soldering process. Aluminum panels were the most difficult to work with because the quality of the solder joint did not easily produce a hermetic seal, however, the bond was strong and consistent otherwise. The results showed promise that with further study a process will be discovered which will make soldering of aluminum more reliable for channel panel assembly. Soldering has most of the advantages of glue, does not degrade greatly over time, and has a stronger bond.

3.2.3 Welding

Welding of the different materials produced more widely varying results than any of the other methods. Several types of welding were attempted they are Gas Tungsten Arc Welding (GTAW), Pulsed and Continuous Nd:YAG Laser, and Resistance Welding. Each of these produced both good and bad results though the GTAW and Resistance welding are more well understood.

GTAW proved very feasible for sealing channel panels due to the ability to penetrate a sufficient depth of material to create a strong and sealed joint. The welding was accomplished manually using both pulsed and unpulsed arcs with equal success. If steel was the material the weld was strong and sealed on the first pass without exception. However, in using aluminum the results varied greatly between a single strong sealed bead to a porous but strong bead. An additional pass was usually

Table 3.2: Gas Tungsten Arc Welding Parameters for Unpulsed (left) and Pulsed (right)

Tungsten Type	Green/Pure	Tungsten Type	Green/Pure
Tungsten Dia.	1/16-3/32	Tungsten Dia.	1/16-3/32
Gas	Argon	Gas	Argon
Flow Rate	30 CFH	Flow Rate	30 CFH
Amps	100-140	Amps	100-140
Polarity	AC	Polarity	AC
Wave Balance	Balance ±20%	Wave Balance	Balance ±20%
Pulse Frequency	N/A	Pulse Frequency	.5-4 Hz
Background Current	N/A	Background Current	20-30 Amps

required to fully seal any assembly. The only control attained over the process was achieved when the parts used were relatively thick. This poses no great problem since the panels can be assembled and then the thickness of the walls reduced as desired afterwords. However, the distortion of the aluminum panels during the welding process is enough to prevent GTAW from becoming the main method in channel panel assembly because most applications of channel panels will require them to be flat.

An autogenous weld was created with a pulsed Nd:YAG laser to seal several blank panels. Aluminum was the material used because copper in general does not weld due to its high reflectivity and thermal conductivity. The process was found to have potential because of the many overlapping uniform weld nuggets. The maximum power and duration were 5 kilowatts and 10 milliseconds which produced 0.010-0.020 inches of penetration in aluminum. The thin welds cracked easily which lead us to the conclusion that the laser unit did not have enough power to achieve the desired penetration. Preheat of the part to enhance the penetration either distorted the part or lead to very little gain in penetration. Powder injection may improve the process but a higher power laser is probably also required to produce the necessary results.

A continuous wave laser was also used to see if it could introduce more local melting but with less total heat introduced to the part. No such success was found

however with the continuous laser. Though the power was varied between 300 and 500 watts the aluminum would melt but not flow together to create a proper bond. It is possible that a higher power laser may produces better mixing conditions.

Resistance welding was only briefly studied due to the lack of large machines to perform the tests. The small spot welding machine did not have any controls for any of the parameters. The operator could control how much pressure was applied and the amount of time the part was subjected to power. A constant pressure of about 5lbs on the lever and a time of 0.5-1.5 seconds produced the most consistent weld nuggets. The weld nuggets were overlapped successively around the edge of the panel creating a seal. Since the operator was unable to uniformly space the nuggets to ensure that each nugget overlapped the previous, there was low reliability in the process. For this type of welding a seam or rolling resistance welder would be the preferred means to sealing channel panels.

3.2.4 Conclusion

The most promising methods for the hermetic assembly of metal channel panels are the GTAW, solder, and resistance welding. Gluing remains useful because it is a cheap and rapid method for joining two parts of any material together. During our evaluation it became apparent that the strength of the bond was more important than the ability to seal the joint on the first try. If there were leaks they could be filled by the same process on a new pass once they were found. In brazing the deformation of the parts due to heating proved too difficult to control and the expense in finding and acquiring the proper braze flux for the different materials was too high to attempt a focused effort. It is likely that with some materials brazing would be the preferred joining method and so it should be pursued again at a future date. Further

investigation should be made into applications for all of the three methods above but especially resistance welding. Resistance welding may provide a fast low distortion method for sealing an aluminum panel of various thicknesses making channel panel manufacturing much more affordable. For the present the most reliable panels can be made from soldered copper with soldered fill tubes.

3.3 Channel Panel Cleaning

Channel Panels, like all heat pipes, require that the interior space be free of oils, corrosion and debris in order to function properly and also to satisfy quality control requirements for some customers. The cleaning of Channel Panels is accomplished at several stages of fabrication to ensure thorough cleaning of the individual parts and the interior space especially. In an engineering environment each Channel Panel would be treated individually according to customer requirements, however, a standard and rigorous cleaning procedure is best. The following cleaning procedure was authored by Jason Hansen [22] of Space Dynamics Laboratory.

Channel panel is a self-contained, passive cooling system. Its large surface area with thin cross-sectional area makes it ideal for, but not limited to, use in the aerospace industry. To be used in this industry, and to obtain peak performance, all internal components must be cleaned to a level of Mil-Std 1246C, and pass a non-volatile residue test (NVR). These tests are performed at SDL by a qualified SDL technician following SDL procedures. All cleaning procedures take place in one of SDL's precision cleaning laboratories (PCL). The technician performing the cleaning must wear proper PCL attire - booties, gown, hat, latex gloves, polyethylene gloves, and beard cover (if applicable) - to maintain personal safety and to avoid possible contamination to the channel panel. Isopropyl alcohol (IPA) with a purity of 99.9%

is used in all cleaning processes.

After the channel plate, spacer plate and spacers have been machined to the customers specifications, they may have machining cutting/cooling fluids, chips, oils and other contaminants on their surfaces. These contaminantes may have adverse effects on the performance of the channel panel if they are not properly cleaned. All channel panel parts are cleaned using the following procedure described in Pre-Assemly Cleaning.

All parts are taken to the PCL where they are placed on the wet bench. they are all initially sprayed with IPA, using the Millipore spray gun, to remove any large particles. They are then placed in the smallest glass dish in which they fit. The aluminum parts are then cleaned with Chem-Crest 211 cleaner. The cleaner is used as directed on the Chem-Crest label with a 1:10 ratio of cleaner to deionized water. The water and cleaner are separately heated to an approximate temperature of 70-80 Celsius. The cleaner and water are then poured over the pieces in the glass dish. They are then placed in an ultrasonicating sink and ultrasonicated for five (5) minutes. The solution is then pured into an appropriate chemical waste container to be disposed of properly at a future time. The parts and glass dish are then rinsed with deionized water and then rinsed again with IPA. The parts are replaced back into the glass dish and immersed in IPA and again ultrasonicated for five (5) minutes. When removing parts from the IPA, polyethylene gloves are used over the latex gloves to eliminate the risk of a contaminating residue that may be left from latex gloves coming in contact with IPA. The parts are then sprayed off with IPA using the Millipore sprayer. The process of ultrasonicating the parts in IPA is repeated four (4) more times. After their final cleaning in IPA, the are dried off by blowing dry nitrogen on all surfaces of each part. They are then sealed in nitrogen filled polyethylene bags to await assembly.

During the assembly process, particles and contaminates may have entered in

to the channel panel chamber. These contaminates may have adverse effects on the performance of the channel panel. The assembled channel panel unit is cleaned using the following procedure described in Post-Assembly Cleaning.

The channel panel is taken to the PCL where the internal chamber may be cleaned out. One of the tubes is hooked up to a flushing assembly. The channel panel is then placed in the ultrasonicating sink and ultrasonicated for five (5) minutes. Deionized water is run through the channel panel for while it is being ultrasonicated. The flushing assembly is then filled with IPA and the channel panel is again ultrasonicated for five (5) minutes while the IPA is run through it. The flushing assembly is then filled with one (1) liter of IPA which is run through the channel panel and collected. This collection of IPA is used to obtain a particle count and perform a NVR.

After the channel panel has been cleaned, it is then placed in a vacuum oven where the remaining IPA is baked out for 24 hours at a temperature of 50 degrees Celsius and a pressure of approximately 0.2 m Torr.

During the filling process, extra care is taken to keep the channel panel clean. However, after the channel panel is filled and sealed, it may have picked up oils dust, etc. To ensure that the channel panel meets the customer's requirements for cleanliness, then channel panel is given a final cleaning. The procedure is described in 3.3.

The sealed channel panel is placed on the wet bench in the PCL and initially sprayed with IPA, using the Millipore spray gun, to remove any large particles. It is then placed in the smallest glass dish in which it will fit. The channel panel is then cleaned with Chem-Crest 211 cleaner. The cleaner is used as directed on the Chem-Crest label with a 1:10 ratio of cleaner to deionized water. The water and cleaner are separately heated to an approximate temperature of 70-80 Celsius. The

cleaner and water are then pured over the channel panel unit in the glass dish. It is then placed in an ultrasonicating sink and ultrasonicated for five (5) minutes. The solution is then pured into an appropriate chemical waste container to be disposed of properly at a future time. The channel panel and glass dish are then rinsed with deionized water and then rinsed again with IPA. The channel panel is placed back into the glass dish and immersed in IPA and again ultrasonicated for five (5) minutes. When removing the channel panel from the IPA, polyethylene gloves are used over the latex gloves to eliminate the risk of a contaminating residue that may be left from the latex gloves coming in contact with IPA. The channel panel is then sprayed off with IPA using the Millipore sprayer. The process of ultrasonicating the parts in IPA is repeated four (4) more times. On the final cleaning, the IPA is collected so that a particle count and NVR may be obtained. The channel panel is removed from the IPA and is dried off by blowing dry nitrogen on all surfaces of the channel panel unit. The channel panel unit is then double bagged in nitrogen filled polyethylene bags.

3.4 Charging Procedure

Channel panels, like all heat pipes, require that the hollow space inside the panel is occupied by a pure working fluid free of non-condensible gases and other fluids which could inhibit the motion of the working fluid. The charging of channel panels is accomplished at the final stage of fabrication to ensure that a pure working fluid is inside the panel. In an engineering environment each channel panel would be treated individually according to customer requirements, however, a standard charging procedure is best. The following charging procedure was authored by Devon Dalton [23] of Space Dynamics Laboratory. For brevity some sections which can be found in the cleaning procedure are not included here.

In order to charge the panel properly with a pure working fluid, the panel must first be emptied of all other substances. If these substances are not emptied, the panel will either cease to work, or not work as well as it could. Substances change the pressure inside the panel, which is the driving force for the panel to operate. They can also block the working fluid from reaching the condenser, which will cause dry out.

The panel is tipped on one end with at least one valve downwards and open to drain. A container is put under the bottom valve to catch whatever fluid is inside because this liquid may be usable. Heat is applied to evaporate the liquid and cause it to push itself out of the chamber. Since the valve is open and gravity is assisting most of the liquid will simply drain through the valve. A syringe is attached to the top valve and used to push the liquid out of the panel. This is repeated ten times, each time removing the syringe, pulling it open and re-attaching it to the panel. The bottom valve is then closed and the syringe is re-attached with all of the air already pushed out of the syringe. The syringe is then pulled open to create a vacuum inside of the panel. Close the valve attached to the syringe, re-close the syringe and attach it again. Open the valve and pull the syringe open again. This is repeated five times. Both valves are then opened and the panel is put on a heat pad set to $125°C$ for one hour. One of the valves is then closed and a vacuum pump is attached to the other valve. The vacuum pump is left on for five minutes. The valve with the pump is then closed and the pump is turned off. Once the valve is closed, the pump can be un-attached to the panel. The channel panel is now ready to be charged.

After a fill percentage is determined using the liquid height calculated in section 1.2 and a syringe is filled with the desired volume of liquid. Attache the syringe to a valve and then open the valve so that the liquid is drawn into the panel by the vacuum inside. Once the liquid has been completely drained from the syringe close

all the valves and remove the syringe. If the liquid is not drawn into the panel by the vacuum inside then the panel has a leak and must be returned to fabrication to fix the leak, clean the panel and repeat the procedure detailed here. This back-filling procedure is the simplest method for charging a channel panel.

Chapter 4

Design

The design of channel panels can be a complicated process if all of the discussed steps and considerations are performed. The level of attention to each should be weighed against the importance of the project. The methods and principles discussed in the previous chapters are intended to be used at the initial levels of design with more sophisticated computer models and experiments to follow in subsequent design phases. In order to communicate the usefulness of FPHP's to a customer a few concise measures of performance are typically reported. Since a FPHP is a two-phase device and both convection and conduction are at work these measures of performance are termed "effective" or "equivalent" for the volume of the FPHP. The values are calculated from the geometry of the FPHP, the heat load, and the expected temperature distribution but depending on which lengths and areas are used and the location of the temperature measurements these measures of performance can vary wildly making the meaning of these "effective" values subjective. Some FPHP's have been experimentally shown to handle heat fluxes of $75\frac{W}{cm^2}$ while others only $3\frac{W}{cm^2}$ and yet the materials, construction and liquids used are the same. Some intuitive considerations of the size of FPHP's can help to explain how some FPHP's seem to outperform others without an appreciable change in methods or materials.

4.1 Practical Matters

The effective or equivalent conductivity k_{eff} of a heat pipe has been a useful tool

for evaluating the performance of the devices in many situations where the movement of the heat can be idealized as one-dimensional. With FPHP's however the spreading of the heat in two dimensions makes k_{eff} a weak description of the performance and so an equivalent convective heat transfer coefficient or overall heat transfer coefficient h_{eq} or U should be used. However even h_{eq} contains some ambiguity. The reasons for this were discussed in Section 2.2.1. A great deal of effort was invested in finding a standard interpretation which would accurately describe the results of the tests performed on channel panels but no defensible results were found. The concept of a single equivalent value which describes the heat transfer capabilities of a FPHP is not useful for clearly communicating the performance of a FPHP.

Some FPHP's are able to handle higher power densities than a similar FPHP made with the same materials, wick structure, and working fluid, but are a different size. This is related to the pressure and the distance which the liquid must travel to return to the evaporator L_{eff}. The higher heat fluxes cause the temperature of the working fluid to rise above its atmospheric boiling point where the pressure begins to rise more quickly as more power is added. FPHP's with a small width and length are able to handle higher power densities because the total pressure on the walls of the FPHP is not as large as with the larger FPHP of the same material, working fluid, and capillary geometry, at the same heat flux. The higher pressure will break the joints made to assemble the FPHP before higher fluxes can be reached.

The capillary limit for small FPHP's does not fail the pipe as quickly. In Equation 1.6, L_{eff} appears in the denominator where as it shrinks the capillary limit grows. The entrainment limit will also be avoided because the vapor will travel a very short distance before it is condensed again and little friction should develop between the vapor and liquid. If the Q_c is sufficiently high the boiling limit will become more dominate, which for any reasonably conductive wall material should be close to the

critical heat flux of the liquid in shallow pool boiling. At any constant temperature the maximum deliverable mass flow rate of liquid to the evaporator by the capillary structure is constant. The actual mass flow rate is dependant upon power input and will increase with power until the maximum mass flow rate is reached; this is called the capillary limit. Refering to the boiling limit Equation 1.9, there is a similar situation at the nucleation sites in boiling. The maximum deliverable mass flow rate of liquid to the nucleation sites in the evaporator is constant. However, the mass flow rate exiting the nucleation site is controlled by the saturation temperature of the liquid, and the thermal resistance of the wall material. This mass flow rate off the evaporator surface increases with the heat flux rather than heat rate making the boiling limit sensitive to heat flux. To summarize and clarify, FPHP's which are capillary limited will reach the capillary limit at a given heat rate or power but FPHP's which are boiling limited will reach the limit at a given heat flux. Therefore it makes sense to report the capillary limit in terms of $Q(Watts)$ and the boiling limit in terms of $Q\frac{Watts}{Area}$.

The goal is to use these considerations to produce believable and understandable measures of performance for channel panel FPHP's. Some of these issues can be overcome by improved construction methods and/or other innovative technologies. The following list is a summary of the issues discussed above:

- Strength of wall material and joints prevents large FPHP's from performing at same power densities as small FPHP's.
- Small FPHP's have a higher capillary limit.
- Small FPHP's are more likely to be boiling limited.

- Each standard FPHP design should have empirical data which can provide power vs. temperature and heat flux vs. temperature as well as an average heat transfer coefficient for each wall material-working fluid combination.

4.2 Conceptual Channel Panel Design

The initial phase of channel panel design uses the tools collected and developed in Chapter 2 and Chapter 3. Other types of FPHP's can be designed in a similar manner by applying the proper operation limit equations (see [2]) and the other correlations identified here. To begin channel panel design candidate wall materials and liquids should be chosen based on the issues discussed in Chapter 3. The required properties are input into the Hubbard-Harris model and a panel geometry iterated on until the desired range of limits is found. The Hubbard-Harris model can include the effect of the liquid height on the limits by subtracting the liquid depth from the available interior thickness to arrive at the actual thickness of the vapor space. The CHF equations for shallow pool boiling are applied to find h_{boil} and also to identify the critical height H_c. From these values the performance of a FPHP can be predicted at various power inputs. Following this the design can be refined and improved for any specific application by using the actual size of the heated zone and power input. Then the joint between the heat source and the FPHP can be modeled using the correlation from Bahrami et al. [20] This ends the initial design phase for FPHP's. Following the initial design various values will be known which can be used to create computer models of the FPHP where all the parameters can be combined into a single solution for the temperature distribution. Prototypes can be made and the model adjusted to fit what was physically achievable during fabrication.

Chapter 5

Conclusion and Recommendation

5.1 Conclusion

In the electronics industry new technologies are rapidly increasing in capabilities while decreasing in size; Even more rapidly in the aerospace industry, demand continues to grow for new spacecraft built with advanced materials and instruments with high thermal sensitivity. It is a constant challenge to make thermal management systems that can handle the heat loads produced by these devices. As the technology develops, flat plate heat pipes may accommodate the higher heat fluxes for these markets. The design of channel panels can be completed with reasonable certainty of achieving the desired results. The following is a summary of the chapter conclusions.

Chapter 1

- The design of FPHP's in general has not been directly addressed in open literature though the phenomena controlling their operation has been studied in detail.

Chapter 2

- The maximum temperature and heat transfer coefficient of the panel are affected by the height of the liquid in the channels. But it is unclear whether this is related to the curvature of the meniscus.

- The Hubbard-Harris model has been shown to accurately predict the operating limits for heat transfer through a channel panel heat pipe at the correct saturation temperature.
- For any channel panel with a constant cooler temperature there is a lower limit to the usefulness of the channel panel as a heat transfer device.
- Boiling in FPHP can be analyzed as a semi-infinite plate.
- Channel panels increase the CHF limit and decrease the onset of nucleate boiling which results in a larger heat transfer coefficient at lower excess temperatures because channel panels use studs and grooves as the surface geometry.
- From a knowledge of H_c and q_c a charge volume can be chosen to maximize the CHF and/or heat transfer coefficient.
- From H_c and q_c the boiling heat transfer coefficient h_{boil} can be obtained.
- The average heat transfer coefficient obtained from the shallow pool boiling correlations is reasonably accurate.
- The joint resistance model by Bahrami [20] can be used to evaluate the temperature drop across the interface between the channel panel and the heat source.

Chapter 3

- Assembly of channel panels currently can be accomplished most easily with materials which are solderable or joinable by adhesives.
- The most promising methods for the future assembly of channel panels are GTAW, resistance welding, and soldering.

- The requirement that FPHP's are hermetically sealed and compatible with the working fluid result in aluminum or copper and water or alcohols be the materials of choice for channel panels.
- High conductivity plastics and composites should be used where light weight is most important.

Chapter 4

- Strength of the wall material, and joints prevents large FPHP's from performing at same power densities as small FPHP's.
- Small FPHP's have a higher capillary limit.
- Small FPHP's are more likely to be boiling limited.
- Each standard FPHP design should have empirical data which can provide Power vs. Temperature and Heat Flux vs. Temperature as well as an average heat transfer coefficient for each wall material-working fluid combination.

5.2 Recommendations

I recommend the following actions be taken to further improve channel panel technology.

- Explore whether the curvature in the meniscus effects ΔT and T_{max} of a channel panel.

- Explore how a surface can become non-wetting for a given liquid as a function of channel width.
- Improve joining methods using or related to GTAW, resistance welding, and soldering of aluminum.
- Identify computer models useful for the modeling of channel panels.
- Determine accurate approximations for the condensation heat transfer coefficient h_{cond} in the condenser of a FPHP.
- Explore the effect of material, surface preparation, and working fluid on boiling heat transfer.
- Innovate new channel geometries to improve capillary pressure.
- Identify current heat pipe technology that can be replaced by channel panel technology and other applications.
- Explore micro-scale channel panel construction methods, limits, and correlations.
- Study the characteristic time to steady state of a channel panel, and as it relates to materials.
- Study correlations for determining the operating temperature of a FPHP under various boundary conditions.

5.3 Summary of Contributions

Correlations useful and necessary to effectively design and build channel panel FPHP's were determined. Appropriate models for the vapor flow, capillary, and boiling limits were tested and shown to be correct. The selection of materials and working

fluids was addressed with qualitative recommendations drawn from experience. Issues with the fabrication and assembly of channel panel FPHP's were explored. Two prototypes were designed, modeled, fabricated, and tested with each independently verifying the correlations identified in this work to be accurate. I identified important correlations, and improved models for use in channel panel design. The Hubbard model was improved to give the engineer more control over the geometry of the channel panel, and the model was improved to more accurately predict the sonic, viscous, entrainment, capillary, and boiling limits. The lowest limit for two channel panels, of very different materials, was verified by experiment. I incorporated the work of Gu [17] to enable the selection of a charge volume that is calculated from Equations 1.14 and 1.13. Additionally, the critical heat flux calculated by Equation 1.14 can be used to find an average heat transfer coefficient of the evaporator surface that I call h_{boil}. The work of Gu is responsible for the discovery of the relationship between CHF and the liquid height, but it is my contribution to suggest that this H be used to identify a charge volume. I have verified by experiment the conditions where h_{boil} is a valid approximation of the convective heat transfer coefficient for the evaporator surface. I have identified a joint resistance model that can be used to model the interface between any channel panel and the system that incorporates the channel panel. The authors of the joint resistance model have performed sufficient study to establish that model as accurate. My conclusion in regard to the joint resistance model is that it is appliable to channel panel-heat source(or cold sink) thermal joints because the materials involved in those joints always meet the requirements of the joint resistance model if the thermal management system is operating within its own limits. The possible methods for the fabrication of channel panels are better understood qualitatively so that future efforts may be more focused. This work results in a simple method for the design of a channel panel.

Bibliography

[1] Chi, S. W., 1976, *Heat Pipe Theory and Practice*, Hemisphere, Washington, DC.

[2] Peterson, G. P., 1994, *An Introduction to Heat Pipes – Modeling, Testing, and Applications,* John Wiley & Sons Inc., New York, Chap. 2-4.

[3] Dunn, P. D., and Reay, D. A., 1982, *Heat Pipes*, 3rd ed., Pergamon Press, New York.

[4] Faghri, A., 1995, *Heat Pipe Science and Technology,* Taylor and Francis Inc., New York, NY.

[5] Garner, S. D., 1996, "Heat Pipes for Electronics Cooling Applications," http://electronics-cooling.com/articles/1996/sep/sep96_02.pnp, **2** (3).

[6] Hubbard, N., 2001, "Model of a Flat Plate Heat Pipe," Senior thesis, Utah State University, Logan, Utah.

[7] Esarte, J., and Dominguez, M., 2003, "Experimental Analysis of a Flat Plate Heat Pipe Working Against Gravity," Report, Instituto del Frio, CSIC Universidad Publica De Nevarra, Spain.

[8] Avenas Y., Gillot, C., Bricard, A., and Schaeffer, C., 2002, "On the Use of Flat Heat Pipes as Thermal Spreaders in Power Electronics Cooling," IEEE 0-7803-7262-X/02.

[9] Schulz-Harder, J., Dezord, J., Schaeffer, C., Avenas, Y., Puig, O., Rogg, A., and Exel, K., 2005, "DBC (Direct Bonded Copper) Substrate with Integrated Flat Heat Pipe," EMPC **June,** Brugge, Belgium.

[10] Vafai, K., and Wang, W., 1992, "Analysis of Flow and Heat Transfer Characteristics of and Asymmetrical Flat Plate Heat Pipe," Int. J. Heat Mass Transf., **35**, pp. 2087-2099.

[11] Zhu, N., and Vafai, K., 1998, "Vapor and Liquid Flow in an Asymmetrical Flat Plate Heat Pipe: A Three-Dimensional Analytical and Numerical Investigation," Int. J. Heat Mass Transf., **41**, pp. 159-174.

[12] Wang, Y., and Vafai, K., 1999, "Transient Characterization of Flat Plate Heat Pipes During Startup and Shutdown Processes," Int. J. Heat Mass Transf., **43(**15), pp. 2641-2655.

[13] Wang, Y., and Vafai, K., 2000, "An Experimental Investigation of the Thermal Performance of an Asymmetrical Flat Plate Heat Pipe," Int. J. Heat Mass Transf., **43**(15), pp. 2657-2668.

[14] Wang, Y., and Peterson, G.P., 2005, "Investigation of a Novel Flat Heat Pipe," ASME J. Heat Transfer, **127**, pp. 165-179.

[15] Cerza, M., and Boughey, B., 2003, "The Effects of Air Infiltration on a Large Flat Heat Pipe at Horizontal and Vertical Orientations," ASME J. Heat Transfer, **125**, pp. 349-355.

[16] Marcus, B., and Fleischman, G., 1970, ''Steady State and Transient Performance of Hot Reservoir Gas-Controlled Heat Pipes,''ASME Paper, NAS2-5503.

[17] Gu, C., 1996, "Critical Heat Flux of Shallow Pool Boiling and Thermal Characteristics of a Flat Plate Heat Pipe," Ph.D. dissertation, U. of Kentucky, Lexington, Ky.

[18] Williams, B., 1995, *Anthology of Applied Thermodynamics Volume I*, Utah St. Univ., Logan, Utah, Chap. 5.

[19] Stephan, P., and Brandt, C., 2004, "Advanced Capillary Structures for High Performance Heat Pipes," Heat Trans. Engin. **25**(3), pp. 78-85.

[20] Bahrami, M., Yovanovich, M., and Marotta, E., 2006, "Thermal Joint Resistance of Polymer-Metal Rough Interfaces," ASME J. of Electronic Packaging, **128**(3), pp 23-29.

[21] Fuller, J., and Marotta, E., 2001, "Thermal Contact Conductance of Metal/Polymer Joints: An Analytical and Experimental Investigation," J. Thermophys. Heat Transfer, **15**, pp. 228–238.

[22] Hansen, J., 2007, "Channel Panel Cleaning Procedure," Space Dynamics Laboratory, Logan, Utah.

[23] Dalton, D., 2007, "Channel Panel Filling Procedure," Space Dynamics Laboratory, Logan, Utah.